1-1-2023

Inelastic behavior of steel and composite frame structure subjected to earthquake loading

P. D. Gajbhiye

Nuha S. Mashaan
Edith Cowan University

V. Bhaiya

Rajan L. Wankhade

S. P. Vishnu

10.3390/applmech4030047
Gajbhiye, P. D., Mashaan, N. S., Bhaiya, V., Wankhade, R. L., & Vishnu, S. P. (2023). Inelastic behavior of steel and composite frame structure subjected to earthquake loading. Applied Mechanics, 4(3), 899-926. https://doi.org/10.3390/applmech4030047

applied mechanics

Article

Inelastic Behavior of Steel and Composite Frame Structure Subjected to Earthquake Loading

P. D. Gajbhiye [1], Nuha S. Mashaan [2,*], V. Bhaiya [3], Rajan L. Wankhade [4,*] and S. P. Vishnu [3]

[1] Department of Civil Engineering, Sardar Vallabhbhai National Institute of Technology, Surat 395007, India; gparam786@gmail.com
[2] School of Engineering, Edith Cowan University, Joondalup, WA 6027, Australia
[3] Civil Engineering Department, Sardar Vallabhbhai National Institute of Technology, Surat 395007, India; vishisht@amd.svnit.ac.in (V.B.); greenhutvishnu@gmail.com (S.P.V.)
[4] Applied Mechanics Department, Government Polytechnic, Bramhapuri 441206, India
* Correspondence: n.mashaan@ecu.edu.au (N.S.M.); rajanw04@gmail.com (R.L.W.)

Abstract: Steel construction is used more often these days as an alternative to the R.C.C. when lightweight, high-strength, large-span structures with a faster erection are required. Extensive studies have been conducted by researchers to study the seismic performance of reinforced concrete and steel structures, both in terms of elastic and inelastic behavior. Composite construction is also a recent advancement in the building industry with similar advantages. However, no emphasis has been given to the comparison between the inelastic behavior of steel and composite structures when subjected to lateral loads. This study compares the inelastic behavior of steel and a composite frame designed to have the same plastic moment capacity for structural members. The responses, such as the formation of hinges, story drifts, story displacements, lateral stiffness, ductility, maximum strength, energy dissipated, joint accelerations, and performance points, are compared with the aid of the building analysis and design software ETABS-18. For this, response spectrum analysis, pushover analysis, and nonlinear direct integration time history analysis have been performed on both frames. For design and analysis, international codes, such as IS 800-2007, IS 875 (Part I, II, IV), IS 1893-2002, AISC 360 (16 and 10), and FEMA 440, have been used. Part of this study also aims at comparing the response of these frames when subjected to near-field and far-field earthquakes. It can be concluded from the results that the post-yield performance of the composite frame is superior to that of the steel frame when seismically excited.

Keywords: direct integration time history analysis; response spectrum analysis; pushover analysis; near-field earthquake; far-field earthquake; ETABS

Citation: Gajbhiye, P.D.; Mashaan, N.S.; Bhaiya, V.; Wankhade, R.L.; Vishnu, S.P. Inelastic Behavior of Steel and Composite Frame Structure Subjected to Earthquake Loading. *Appl. Mech.* **2023**, *4*, 899–926. https://doi.org/10.3390/applmech4030047

Received: 23 May 2023
Revised: 5 July 2023
Accepted: 25 July 2023
Published: 16 August 2023

1. Introduction

Composite in the construction industry is a word that refers to the usage of steel, reinforced concrete, and composite steel–concrete components in combination with one another. Mixed or hybrid systems are a contemporary trend in the building sector. These structures maximize the structural and economic advantages of each component type by optimizing their usage. Thorough research is presently being performed to have a better grasp of how such frames operate. On the other hand, a beam–column combination has long been known for its better earthquake protection and has become a popular building method. In light of the growing popularity and usage of such systems, frame analysis is required. Additionally, nonlinear analysis is a strong tool for better understanding system behavior, especially when dynamic excitation occurs. Available analytic programs are capable of simulating the behavior of typical steel or composite structures. In the past, powerful earthquakes have caused major property damage and fatalities. Earthquake damage is primarily related to seismically weak buildings, which were frequently constructed prior to the adoption of modern building rules. As a result, academics have concentrated their

efforts on discovering novel and effective ways to mitigate seismic risk in such structures. Direct-integration THA is a nonlinear, dynamic analysis method in which the structure is subjected to seismic load varying with respect to time, and the equilibrium equations of motion are integrated fully to obtain the response of the structure. This is achieved by integrating structural characteristics and behaviors for successive time steps that are very short compared to the seismic excitation period. The equation of motion used in this method is

$$Mu''(t) + Cu'(t) + Ku(t) = F(t) \quad (1)$$

Pushover analysis is a nonlinear static approach in which a predetermined pattern gradually increases the magnitude of structural loads along the lateral direction of the structure. The behavior of the structure is generally believed to be governed by its fundamental mode, and the predefined pattern is expressed in either story shear or fundamental mode shape. The displacement control raises the displacement of the building's top story so that the building is subjected to the required level of horizontal load. The distance to which the structure is pushed is proportional to its fundamental horizontal mode of translation. In both kinds of pushover analysis, the structure's stiffness matrix may need to be changed for each increase in load or displacement when it changes from elastic to inelastic. Usually, the displacement-controlled pushover analysis is favored over the force-controlled pushover analysis as the research may be performed to the desired level of displacement.

A number of research works have been carried out in the field of seismic analysis of steel and composite frames, and the effects of various parameters on the seismic behavior of the structure are, hence, known. The inelastic behavior of frames is well possible with respect to the performance-based design [1]. Hence, we can access response-based damage of structures more effectively [2–4]. Chopra [5] provided comparing response of SDF Systems to Near-Fault and Far-Fault Earthquake Motions in the Context of Spectral Regions. For inelastic structures, a displacement-based seismic design procedure is also available, which can be more effectively used [6]. Some light is also put on correlation study between seismic acceleration parameters and damage indices of structures [7]. Indian design codes are also given provisions for the analysis and design of such structures [8,9]. In structural frames with steel-concrete composite columns subjected to axial and flexural loading performance changes abruptly [10]. In this regards Indian code is useful to consider steel and ductile design [11]. For more effective design and analysis, cross-sectional properties of complex composite beams need to be obtained [12]. A friction-tuned mass damper can also be used for statistical linearization of such frames [13]. Further, we obtain the literature on the assessment of minimally compliant low-rise base-isolated and conventional steel moment-resisting frame buildings [14]. Different types of bracings are required to improve the performance of ductile frames [15]. A performance-based design approach is more useful for better estimation of forces and design of structural elements [16–19]. Additionally, optimum positioning of shear walls is also treated as remedial measures to mitigate the effects of lateral forces in building frames [20]. We can investigate the in-plane flexibility of steel-deck composite floors in steel structures for a more effective design approach [21]. Connections play a major role in the performance assessment of steel frames [22]. Experimental, analytical, and numerical estimation is required for composite frames [23]. Seismic Fragility of Buildings under earthquake impact is necessary to better understand the forces [24]. Some studies also discussed the effects of dissipative systems on the seismic behavior of irregular buildings, which also depends upon the stiffness in the main direction in building frames [25,26]. Super-elastic SMA-bolted connection is also preferred for assessing the performance of the equipped structures [27]. H-shaped composite beam–columns in composites are required to be studied for the uniaxial and biaxial compressive behavior [28].

2. Methodology and Structural Description

In this study, two G + 10-story frames, steel, and a composite frame, are considered for comparison. Both frames have a floor-to-floor height of 3 m and three bays of 5 m

each in both directions of the plan. The supports are fixed at the base and rest on Type-II (medium) soil. A damping of 5% and an importance factor of 1 is assumed. Modal analysis, response spectrum analysis, and pushover analysis are performed to assess the vulnerability of building frames. Direct integration time history analysis is also performed for the comparison of the results.

For columns, structural steel Fe345, for beams, structural steel Fe250, concrete of grade M30, rebars of grade Fe415, deck slab material Fe250, and shear studs of grade Fu400 have been used. The plan and 3-dimensional view of the completed model is shown in Figure 1. The types of sections used in this study are shown in Figure 2. Encased column section is used in the composite frame, and the hot-rolled steel section is used as a column in a steel frame. For both frames, hot-rolled steel sections are used for primary and secondary beams. Deck slab assembly with shear studs is used in both frames. All the sections are designed to have the same plastic moment capacity. For all sections other than the composite column, the following equation is used to calculate the plastic moment capacity:

$$M_p = Z_p \times f_y \tag{2}$$

where Zp is a plastic section modulus and fy is yield stress of the material. For the composite column, the SAP2000 design modeler has been used to calculate the plastic moment capacity by Caltrans idealization of the M-ϕ (moment-curvature) curve.

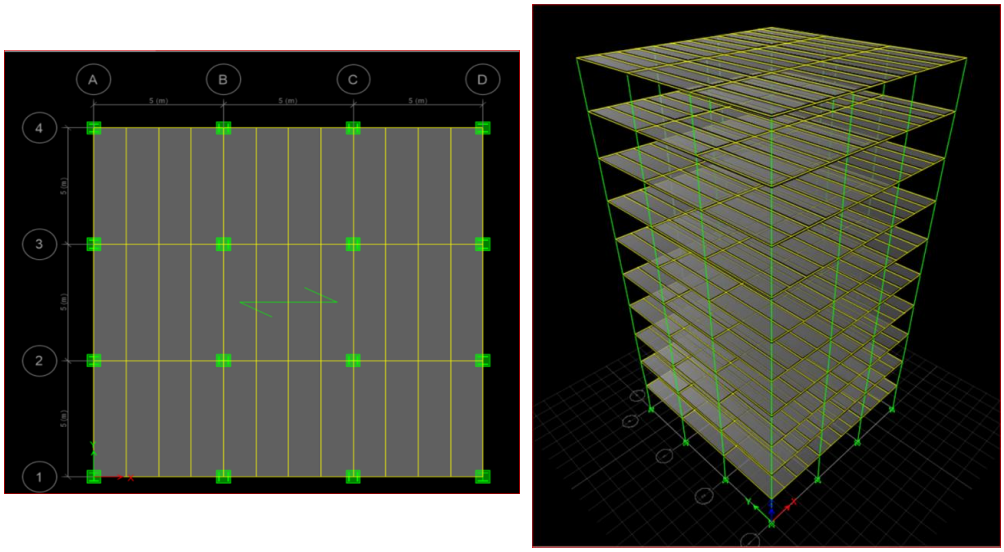

Figure 1. Plan and elevation of a building frame.

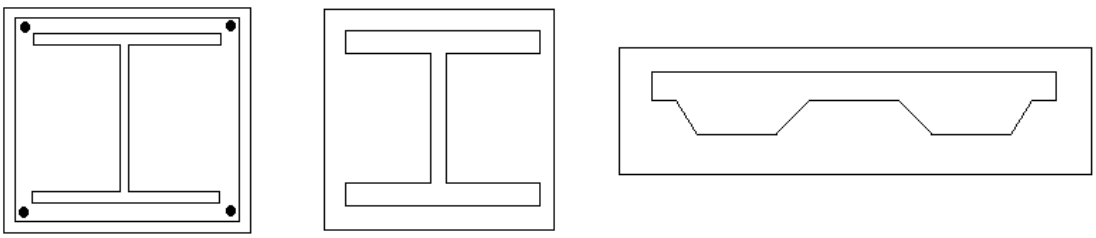

(**a**) (**b**) (**c**)

Figure 2. (**a**) Encased Section; (**b**) Steel Section; and (**c**) Deck slab section for composite frame.

3. Load Details and Design Sections

The dead, live, and seismic loads were assumed as per IS 875: Part 1, 2:1987 and IS 1893: Part1:2002. Self-weight, an imposed load of 2.5 kN/m^2, floor finish of 1.5 kN/m^2,

roof live load of 1.5 kN/m^2, and wall load of 6 kN/m (brick density = 22 kN/m^2) is applied on the frames. For equivalent static analysis, seismic zone factor 0.36, Site type-II, importance factor 1, response reduction factor 5, and damping of 5% have been assumed. Fourteen load combinations are considered in the design in accordance with IS 1893:2016. The steel frame design is made in accordance with IS 800:2007, the composite beam design in accordance with AISC 360-16, and the composite column design in accordance with AISC 360-10. The sections are chosen so that the plastic moment capacities are the same for both steel and composite frame. The load combinations considered are as follows:

$$\begin{aligned}
&\text{Dead load, Live load :} && 1.5\,(\mathrm{DL}+\mathrm{LL})\\
&\text{Dead load, Live load and Seismic load :} && 1.2\,(\mathrm{DL}+\mathrm{LL}+\mathrm{EQx})\\
&\text{Dead load, Live load and Seismic load :} && 1.2\,(\mathrm{DL}+\mathrm{LL}-\mathrm{EQx})\\
&\text{Dead load, Live load and Seismic load :} && 1.2\,(\mathrm{DL}+\mathrm{LL}+\mathrm{EQy})\\
&\text{Dead load, Live load and Seismic load :} && 1.2\,(\mathrm{DL}+\mathrm{LL}-\mathrm{EQy})\\
&\text{Dead load, Seismic load :} && 1.5\,(\mathrm{DL}+\mathrm{EQx})\\
&\text{Dead load, Seismic load :} && 1.5\,(\mathrm{DL}-\mathrm{EQx})\\
&\text{Dead load, Seismic load :} && 1.5\,(\mathrm{DL}+\mathrm{EQy})\\
&\text{Dead load, Seismic load :} && 1.5\,(\mathrm{DL}-\mathrm{EQy})\\
&\text{Dead load, Seismic load :} && 0.9\mathrm{DL}+1.5\mathrm{EQx}\\
&\text{Dead load, Seismic load :} && 0.9\mathrm{DL}-1.5\mathrm{EQx}\\
&\text{Dead load, Seismic load :} && 0.9\mathrm{DL}+1.5\mathrm{EQy}\\
&\text{Dead load, Seismic load :} && 0.9\mathrm{DL}-1.5\mathrm{EQy}
\end{aligned} \tag{3}$$

In the above, dead load (DL), live load (LL), earthquake load in x direction (EQx) and earthquake load in y direction (EQy) are considered depending upon loads on the building frame. Hence, the analysis was performed for each load case combination as stated above.

The plastic moment capacity of sections after the design is given in Table 1.

Table 1. Plastic moment capacity of sections.

Object		Section	Plastic Moment Capacity, Mp (kN-m)
Column (IS 12778:2004)	Steel	WPB 300 × 300 (237.92 kg/m)	1406.84
	Composite	WPB 360 × 370 (165.34 kg/m) Embedded cross section	1407.27
Primary beam for both frames (IS 800:2007)		ISWB 300 (48.1 kg/m)	182.80
Secondary beam for both frames (IS 800:2007)		ISLB 225 (23.5 kg/m)	63.68

The "Mp" for the composite column was calculated by Caltrans idealization of the M-ϕ curve with the aid of the SAP2000 design modeler. Figure 3 shows the actual M-ϕ curve and the idealized M-ϕ curve. The final sections after static analysis and design in Etabs are WPB 300 × 300 for steel column, WPB 360 × 370 encased 540 × 540 mm M30 concrete with 25 mm dia bars at corners, and 12 mm dia lateral ties with clear cover 40 mm for composite column, ISWB 300 for primary beams and ISLB 225 for secondary beam. For the deck slab, a 1-mm-thick membrane filled with M30 concrete with a slab depth of 110 mm and rib depth of 75 mm. Six shear studs with a height of 150 mm and 19 mm dia are provided on all secondary beams.

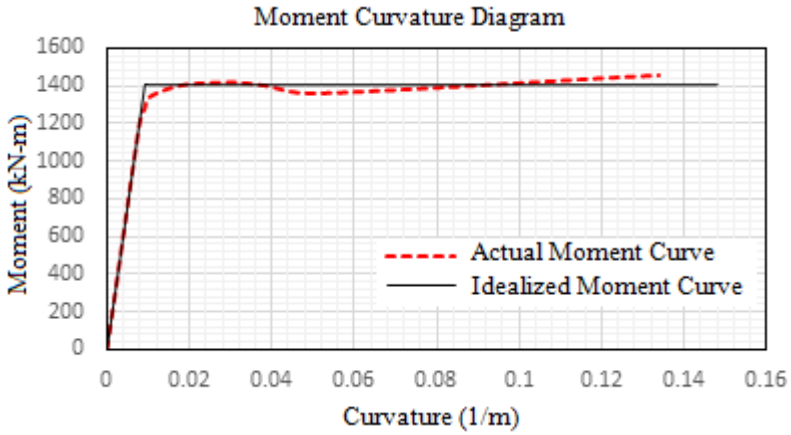

Figure 3. Moment curvature curve of composite column section.

The plastic moment capacity of composite columns can be calculated by separate formula. It considers the superposition of the strengths by the steel section and the concrete to develop their individual plastic strengths. As per AIJ (1987) and AISC (1999), the P-M interaction curve to be obtained for the composite column is taken as follows [10]:

$$\text{When}: \quad \begin{matrix} 0 \leq P_u \leq {}_uN_c \\ P_u = C_c \, and \, M_u = M_p + C_c \end{matrix} \tag{4}$$

$$\text{When}: \quad \begin{matrix} P_u > {}_uN_c \\ P_u = {}_uN_c + N_s \, and \, M_u = M_s \end{matrix} \tag{5}$$

In the above equation, ${}_uN_c$ is the axial load capacity of the concrete core when it is not subjected to any moment. M_p is the plastic moment capacity of the steel section. $N_c \, and \, M_c$ are the axial load and moment, respectively, resisted by the concrete core. $N_s \, and \, M_s$ are the axial load and moment, respectively, resisted by the steel section.

4. Results and Discussions

After the static analysis and design of the frames in ETABS, the model has been validated by comparing the manually calculated result and software result of lateral load distribution along the height of the steel frame. The seismic coefficient method has been used as per IS 1893:2002 to do the validation. The results showed only a slight variation of 6%. The validation result is shown in Figure 4. The values are given in Table 2.

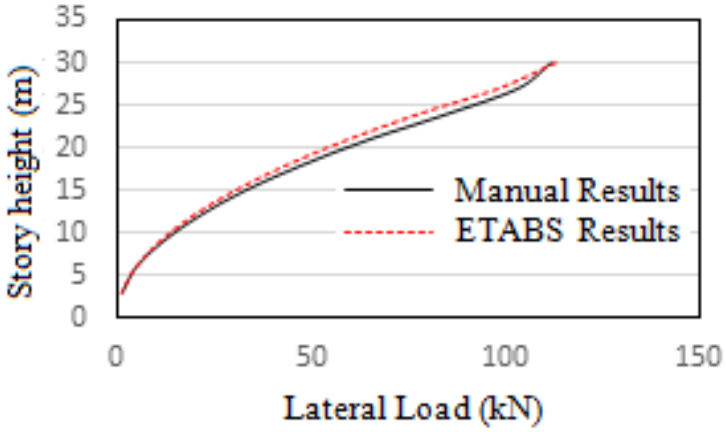

Figure 4. Validation of Lateral load distribution with comparison.

Table 2. Lateral load distribution.

Story	Elevation (m)	Lateral Load Distribution (kN)	
		Software	Manual
Story10	30	112.9491	111.799
Story9	27	98.3869	103.4
Story8	24	77.7378	85.2
Story7	21	59.518	65.01
Story6	18	43.7275	47.77
Story5	15	30.3663	32.99
Story4	12	19.4344	21.17
Story3	9	10.9319	11.82
Story2	6	4.8586	4.925
Story1	3	1.2147	1.329
Σ Total		459.14	492.51

4.1. Modal Analysis

The model in this study does not consider the effects of shear walls, lift well, infill wall effects, and other non-structural elements in the design. Moreover, the sections chosen are larger than the least sections required for optimum design. This is owing to the criteria for comparison of the frames keeping the plastic moment capacity of the assumed sections the same. The column size has been kept constant throughout the building height, which has further increased the design section and overall mass of the frame. Furthermore, the loads applied and the influence of the stiffness of the floor slabs also affect the time period. Considering all these factors, the time period of the modeled frames is a little higher than usual in the 10-story buildings. The time periods of the first three modes are given in Table 3. Modal analysis has been performed via the Ritz analysis method in Etabs, as it provides better results for time history analysis. The natural frequencies obtained for steel and composite frames are 0.40 Hz and 0.44 Hz, respectively.

Table 3. Modal time periods.

Mode	Period(s)	
	Composite	Steel
1	2.189	2.373
2	2.187	2.339
3	1.775	2.001

4.2. Response Spectrum Analysis

Response spectrum analysis was performed for both steel and composite frames in both *x* and *y* directions as per IS 1893:2002 for 5% damping, Soil type II, and seismic zone V. The responses obtained in both directions are similar due to the symmetric configuration of the frames. The comparison of the story displacement, story drift, overturning moment, story shear, and story stiffness are shown in Figures 5–7. The values obtained for maximum top story displacement and story drift are greater for a steel frame. Base shear, story overturning moments, and story stiffness values are greater for the composite frame. The greater base shear and overturning moments of the composite frame are due to higher stiffness. Its lower story drift and displacements are due to better stiffness. The maximum responses of steel and composite frames after response spectrum analysis are given in Table 4.

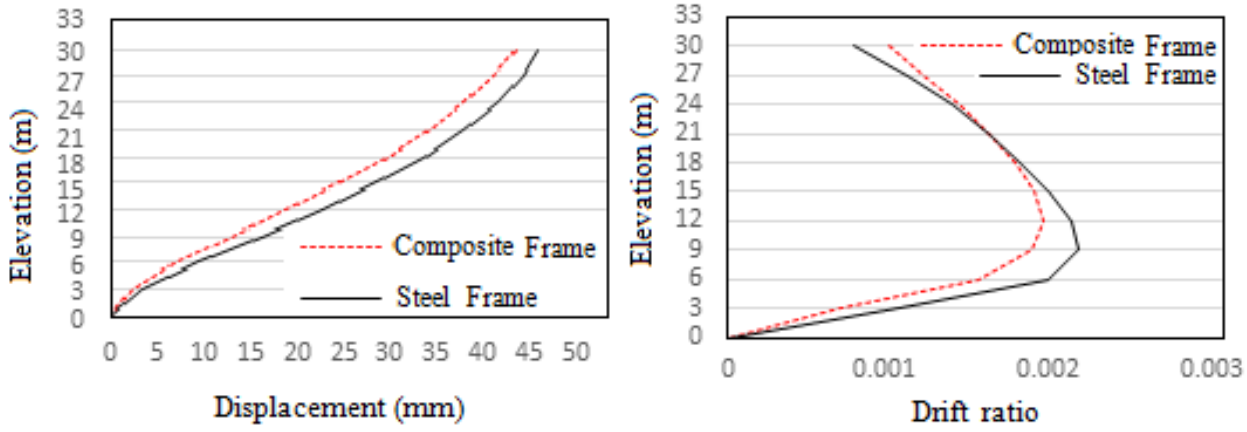

Figure 5. Maximum story displacement and maximum story drift along *x*-axis.

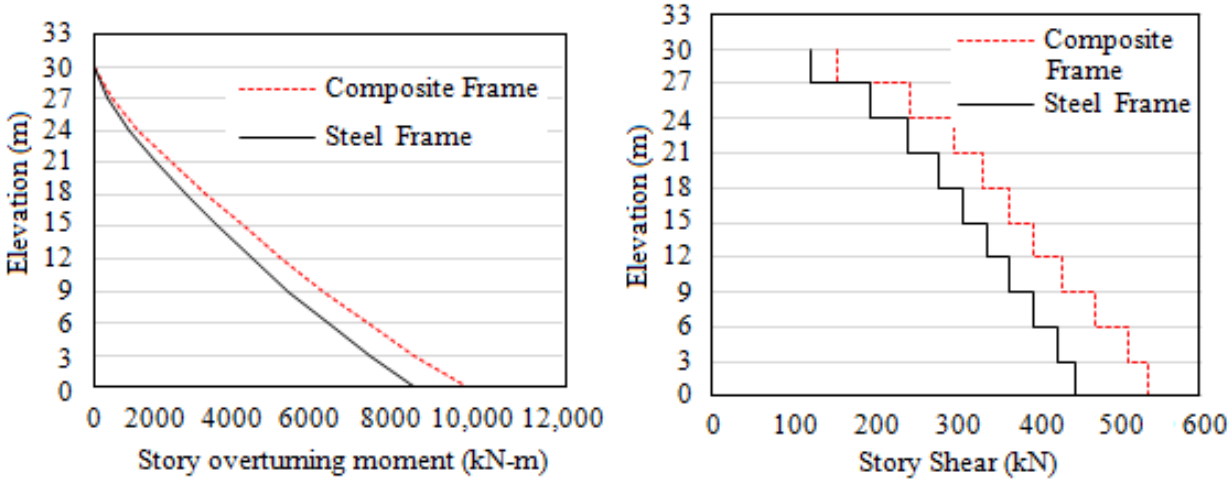

Figure 6. Story overturning moment (kN-m) and story shear (kN) along *x*-axis.

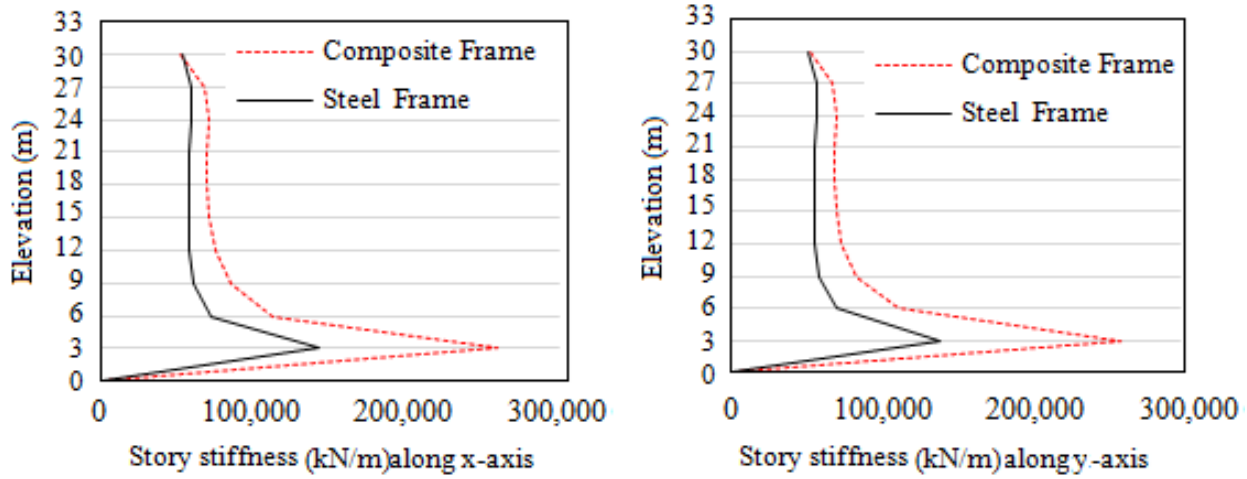

Figure 7. Story stiffness along *x*-axis and *y*-axis (kN/m).

Table 4. Comparison of maximum responses.

Response	RSx		RSy	
	Composite	Steel	Composite	Steel
Maximum story displacement (mm)	41.17	43.43	41.21	43.96
Maximum story drift	0.0019	0.00214	0.0019	0.00216
Story overturning moment (kN-m)	9550.4	8195.9	9541.2	8046.4
Story shear (kN)	533.39	444.41	532.98	437.02
Story stiffness (kN/mm)	259.8	142.7	259.6	140.3

4.3. Pushover Analysis

Since the behavior of the frames is similar in both directions, as evident from the response spectrum analysis due to the symmetric configuration of the frames, pushover analysis is performed only for horizontal *x*-direction. Autohinges were assigned as per AISC 41-13 to both ends of structural members at relative distances of 0.1 and 0.9, respectively. M3 (Flexural) hinges were assigned to beams, and P-M2-M3 (Coupled axial and Biaxial bending) hinges were assigned to the columns. The displacement coefficient method was applied as per AISC 41-13 to obtain the target/maximum displacement using modification coefficients to peak elastic displacement. The pushover curve is used to determine effective stiffness and period, and when used with a response spectrum, gives the spectral acceleration. The spectral acceleration is converted into the elastic displacement, to which coefficients are applied to determine the target displacement. It uses the relation

$$\text{Target displacement, } d = C_0 C_1 C_2 S_a \left(\frac{T_e^2}{4\pi^2} \right) g \tag{6}$$

where C_0 is a factor to relate the spectral displacement of the equivalent SDoF and building roof displacement; C_1 is a modification factor relating expected maximum inelastic displacements to displacements calculated for a linear elastic response; C_2 is a modification factor to represent the effect of hysteresis shape on the maximum displacement response; Sa is the spectral acceleration at the effective period and damping ratio of the building in the direction under consideration; T_e is the effective period of the building in the direction under consideration, and g is the acceleration due to gravity. The capacity spectrum method was utilized as per FEMA 440 equivalent linearization to obtain the performance point by overlapping the capacity spectrum and the design spectrum. A control displacement of 700 mm was applied to the top story joint label 1. P-Delta geometric nonlinearity was also considered in the analysis.

For the steel frame, push-x was run in the steel frame, and the following are the results obtained. Table 5 represents the pushover details in each of the steps.

Table 5. Hinge details of steel frame.

Step	Monitored Displ. (mm)	Base Force (kN)	A-B	B-C	C-D	D-E	>E	A-IO	IO-LS	LS-CP	>CP	Total
0	0	0	800	0	0	0	0	800	0	0	0	800
1	120	1345.5072	800	0	0	0	0	800	0	0	0	800
2	194.075	2176.0667	798	2	0	0	0	800	0	0	0	800
3	244.108	2614.2609	736	64	0	0	0	776	24	0	0	800
4	368.062	3036.3915	678	122	0	0	0	690	110	0	0	800
5	550.505	3395.5062	654	146	0	0	0	656	114	30	0	800
6	572.011	3432.5150	652	146	2	0	0	656	96	48	0	800
7	563.901	3117.8298	652	136	4	0	8	656	94	42	8	800

Figure 8 shows the formation of different safety levels of hinge formation across the pushover analysis. The different safety levels are intermediate occupancy (IO), life safety

(LS), and collapse prevention (CP). IO hinges are shown in green color; LS hinges are shown in light blue color, and CP hinges are shown in red color.

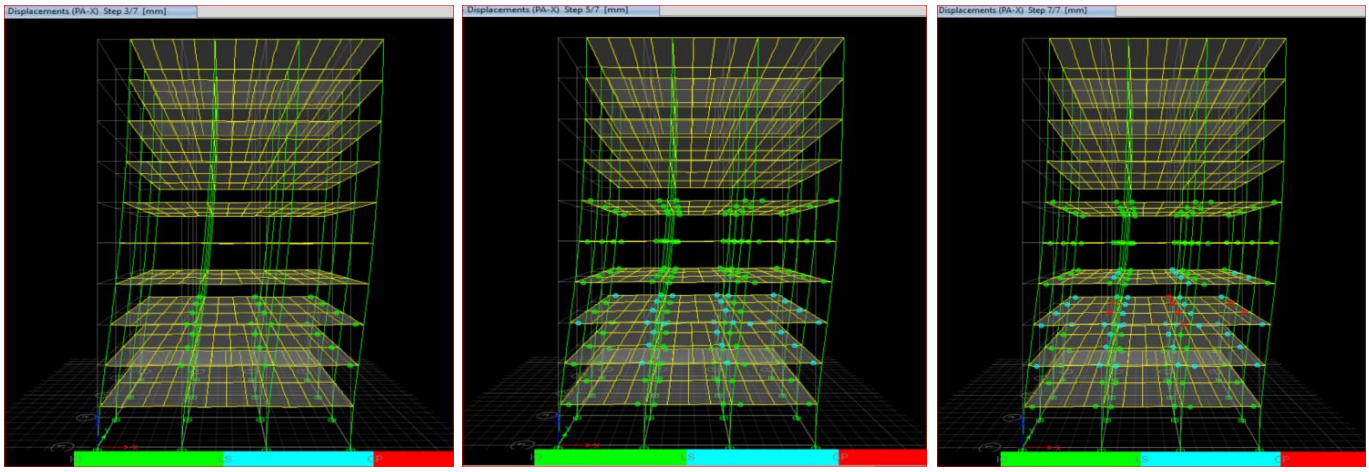

Figure 8. Step 3: IO level hinges; Step 5: LS level hinges; Step 7: CP level hinges.

To obtain the performance point of the steel frame, the IS 1893:2002 for the design-based earthquake was used in the capacity spectrum method. A Damping ratio of 0.05 and scale factor of "g" (acceleration due to gravity) is assumed. The IS design spectrum represented in terms of spectral acceleration vs. time period is converted to the acceleration displacement response spectrum (ADRS) in terms of spectral acceleration vs. spectral displacement. Then, the ADRS curve is overlapped with the capacity curve obtained from the pushover analysis to obtain the required performance point. This gives the performance point of the steel frame for the given site details.

The graph showing the performance point is illustrated in Figure 9. The target displacement calculated according to ASCE 41-13 is shown in Figure 10.

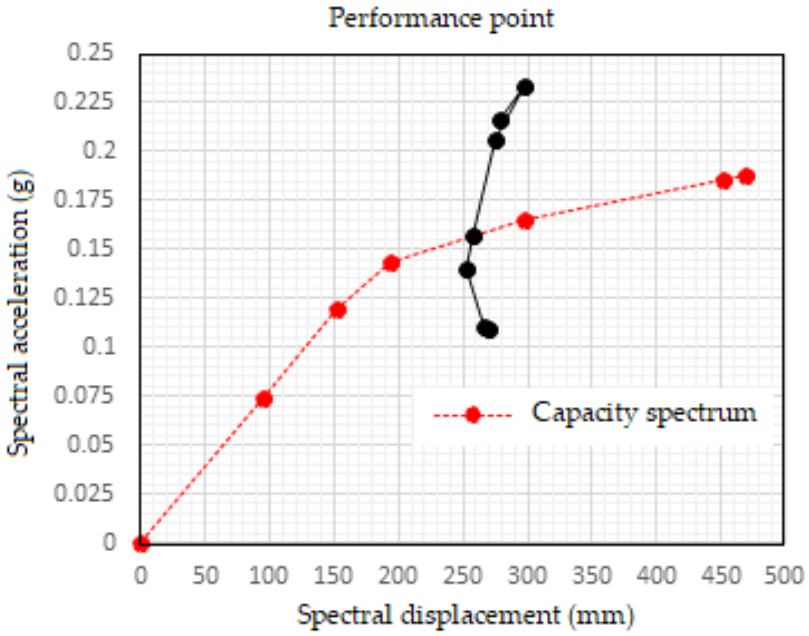

Figure 9. Performance point as per IS1893:2002 for steel frame.

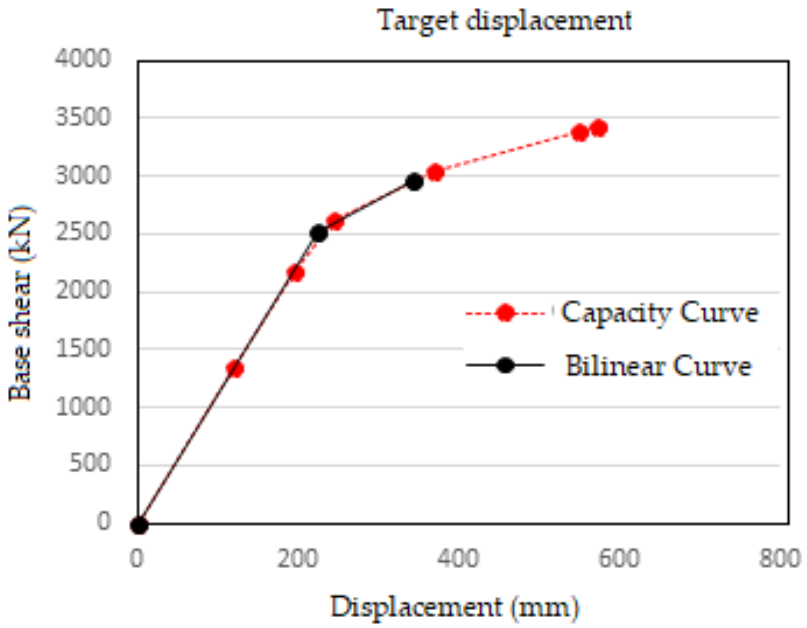

Figure 10. Target displacement as per IS1893:2002 for steel frame.

Composite frame Push-x was run in the composite frame and the following are the results obtained. Table 6 represents the pushover details in each of the steps.

Table 6. Hinge details of composite frame.

Step	Monitored Displ. (mm)	Base Force (kN)	A-B	B-C	C-D	D-E	>E	A-IO	IO-LS	LS-CP	>CP	Total
0	0	0	800	0	0	0	0	800	0	0	0	800
1	120	1713.0875	800	0	0	0	0	800	0	0	0	800
2	204.016	2884.5333	796	4	0	0	0	800	0	0	0	800
3	256.971	3445.6811	716	84	0	0	0	768	32	0	0	800
4	378.584	4078.8834	650	150	0	0	0	680	120	0	0	800
5	472.306	4378.2101	618	182	0	0	0	646	154	0	0	800
6	525.33	4455.5615	616	184	0	0	0	636	164	0	0	800
7	549.436	4473.9862	616	184	0	0	0	624	172	4	0	800
8	596.002	4430.5584	614	174	0	0	12	616	146	38	0	800
9	605.241	4414.625	612	176	0	0	12	616	128	56	0	800
10	614.824	4376.4091	612	176	0	0	12	616	122	62	0	800
11	620.741	4327.1105	612	172	0	0	16	616	120	64	0	800
12	620.753	4327.1298	612	172	0	0	16	616	120	64	0	800
13	628.401	4259.8434	612	172	0	0	16	616	108	76	0	800
14	631.331	4243.5798	612	168	4	0	16	616	106	78	0	800
15	631.343	4061.4931	612	164	2	0	22	616	104	74	6	800
16	633.795	4078.3067	612	162	4	0	22	616	104	74	6	800

We show the formation of different safety levels of the hinge formation across the pushover analysis. The different safety levels are intermediate occupancy (IO), life safety (LS), and collapse prevention (CP). IO hinges are shown in green color; LS hinges are shown in light blue color, and CP hinges are shown in red color.

The performance point and target displacement are found through the same steps as before. The graph showing performance point is illustrated in Figure 11. The target displacement calculated according to ASCE 41-13 is shown in Figure 12.

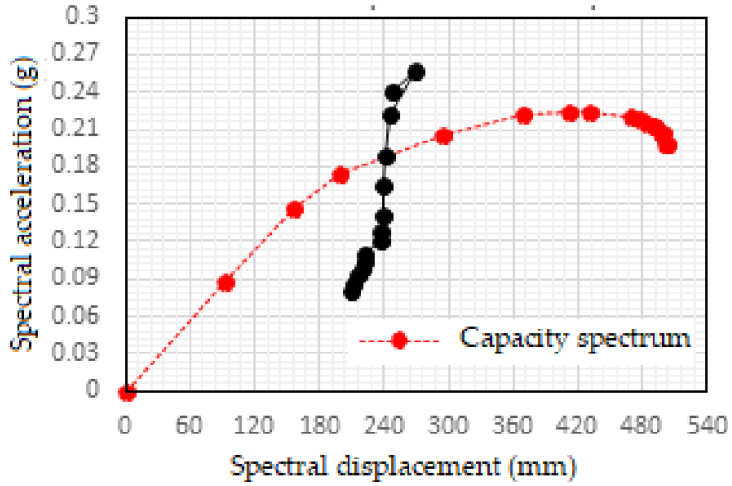

Figure 11. Performance point as per IS1893:2002 for composite frame.

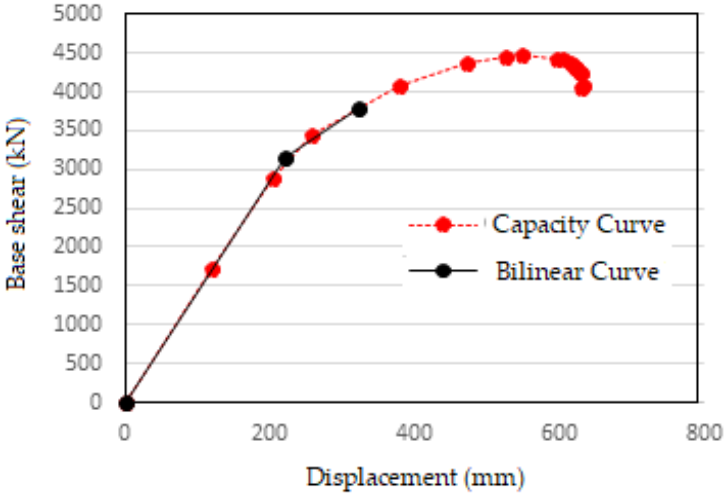

Figure 12. Target displacement as per IS1893:2002 for composite frame.

4.4. Comparison of Performance Point and Target Displacement for Frames

The values of performance point and target displacement for steel and composite frames are compared and shown in Tables 7 and 8. The values obtained by displacement coefficient method are slightly higher than that obtained in capacity spectrum method due to the difference in techniques which is as expected. The results indicate greater shear resistance or base shear values for composite frame whereas greater displacement values are obtained for steel frame for the given IS response spectrum.

Table 7. Comparison of performance points.

Parameters	Performance Point as per FEMA 440 EL	
	Composite Frame	Steel Frame
Shear (kN)	3733.57	2875.25
Displacement (mm)	312.26	320.74
Sa (g)	0.1886	0.1568
Sd (mm)	242.25	257.97
Teff (s)	2.18	2.39

Table 8. Comparison of target displacements.

Parameters	Target Displacement as per ASCE 41-13 NSP	
	Composite Frame	Steel Frame
Shear (kN)	3787.86	2954.46
Displacement (mm)	322.69	344.01

4.5. Comparison of Progressive Hinge Formation in Steel and Composite Frame

The total number of hinges assigned was 800 in both frames. At the time of failure, the steel frame had 656 hinges within immediate occupancy, 94 hinges between immediate occupancy for life safety, 42 hinges between life safety for collapse prevention, and 8 hinges over collapse prevention. Whereas for the same level of loading composite frame had 616 hinges within immediate occupancy, 146 hinges between immediate occupancy for life safety, 38 hinges between life safety for collapse prevention, and no hinges over collapse prevention were formed. The collapse of the composite frame occurred only at a higher displacement load. Figures 13–15 show the number of hinges in each of the safety levels as the frames are pushed in increments of displacement till total collapse.

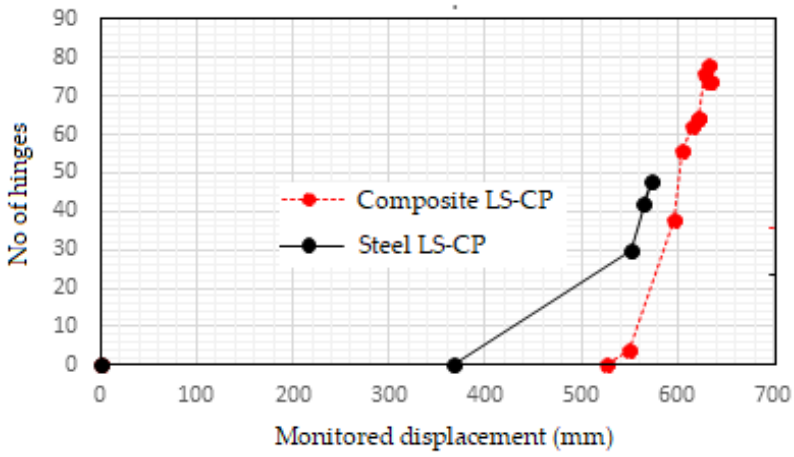

Figure 13. Comparison of monitored displacement.

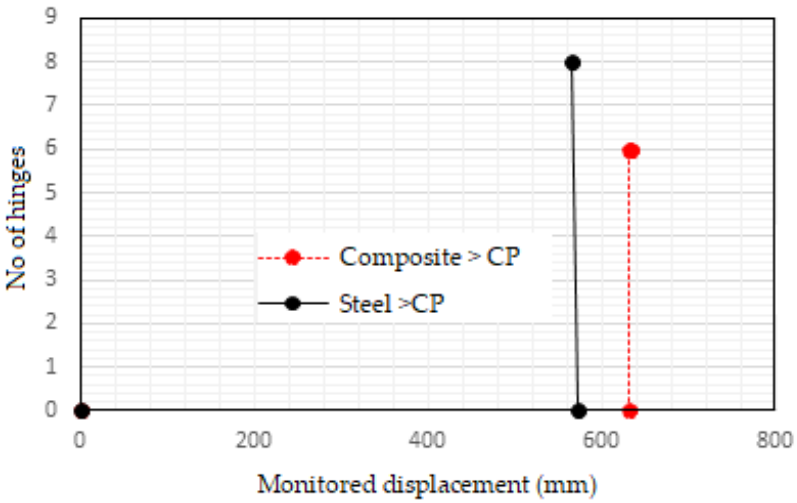

Figure 14. Monitored displacement after collapse.

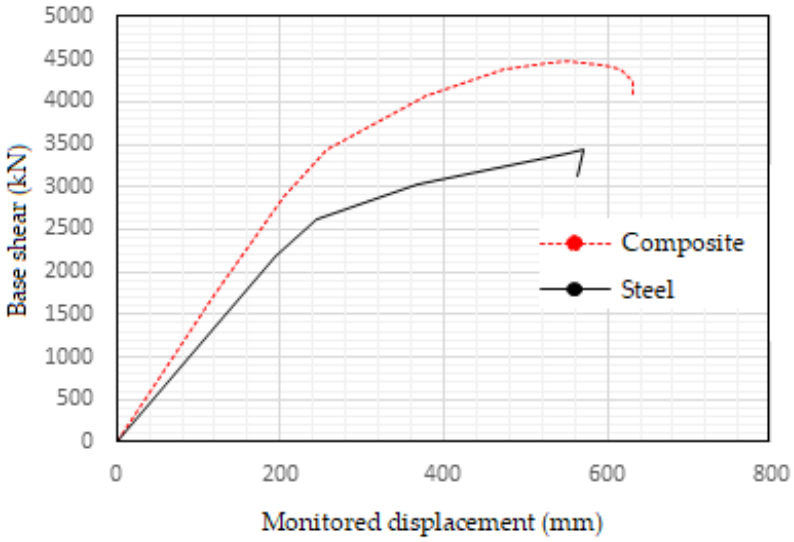

Figure 15. Static pushover curve of steel and composite frame.

As the loading progress beyond a certain displacement, the number of IO-LS hinges is higher for composite frames because the greater number of hinges in steel frames starts changing to LS-CP hinges.

It can be seen from the graph that the same displacement number of LS-CP hinges is greater for steel frame than composite frame since most of the hinges in composite frame still continue to remain in IO-LS level.

4.6. Number of Hinges Crossing the CP Threshold

It is clearly visible in the graph that the number of hinges over the CP level is greater for the steel frame when it fails. At the same displacement load, no hinges over the CP level are formed in the composite frame. The composite frame starts developing hinges over the CP level only at a greater monitored displacement when it fails.

Structural characteristics of steel and composite frame are evaluated. The static pushover curve of steel and composite frame is shown in Figure 15. It shows the lateral resistance vs. deformation of the structures until they reach failure from a global standpoint.

Further, Figure 16 shows the capacity curve idealized according to ASCE 41-13 NSP. The seismic characteristics of both frames can be calculated from these curves. The details of the idealized graph are given in Table 9.

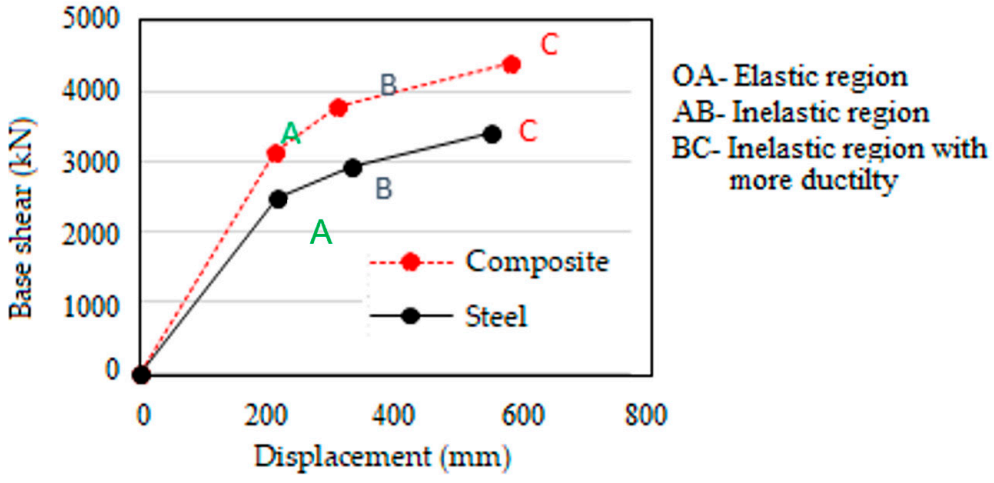

Figure 16. Idealized capacity curve.

Table 9. Idealised curve data.

Region	Ideal Curve Composite		Ideal Curve Steel	
	Displacement (mm)	**Base Shear (kN)**	**Displacement (mm)**	**Base Shear (kN)**
Elastic region	0 220.009	0 3140.79	0 223.709	0 2508.351
Plastic region	322.69 605.241	3787.862 4414.625	344.005 572.011	2954.464 3432.515

From the idealized curve, the overall properties of the frames are calculated as follows:

(i) Global stiffness of the frames:

The stiffness of the frames in various phases is found by taking the slope of the ideal curve.

$$\text{Slope, } M = \left(Y^2 - Y^1\right) / \left(X^2 - X^1\right) \tag{7}$$

(a) Composite frame:

$$\begin{aligned}&\text{Stiffness in the region OA} = 3140.79/220.009 = 14.28\ \text{kN/mm} = 14{,}275.7\ \text{kN/m (Elastic region)}\\&\text{Stiffness in the region AB} = (3787.86 - 3140.79)/(322.69 - 220.009) = 6.3\ \text{kN/mm} = 6301.8\ \text{kN/m (Inelastic region)}\\&\text{Stiffness in the region BC} = (4414.63 - 3787.86)/(605.24 - 322.69) = 2.22\ \text{kN/mm} = 2218.2\ \text{kN/m (Inelastic region)}\end{aligned} \tag{8}$$

(b) Steel frame:

$$\begin{aligned}&\text{Stiffness in the region OA} = 2508.35/223.709 = 11.21\ \text{kN/mm} = 11{,}212.6\ \text{kN/m (Elastic region)}\\&\text{Stiffness in the region AB} = (2954.46 - 2508.35)/(344.01 - 223.71) = 3.71\ \text{kN/mm} = 3708.5\ \text{kN/m (Inelastic region)}\\&\text{Stiffness in the region BC} = (3432.52 - 2954.46)/(572.01 - 344.01) = 2.09\ \text{kN/mm} = 2096.7\ \text{kN/m (Inelastic region)}\end{aligned} \tag{9}$$

(ii) Ductility:

Ductility can be measured as the ratio of maximum deformation to the idealized yield deformation.

$$\text{Ductility, } \mu = \Delta\text{max}/\Delta\text{y}$$

(a) Composite frame:

$$\mu = 605.24/220.009 = 2.75$$

(b) Steel frame:

$$\mu = 572.011/223.709 = 2.56 \tag{10}$$

(iii) Lateral strength:

It is the maximum resistance that the structure offers during the entire history of resistance vs. deformation.

(a) Composite frame:

$$\text{Maximum strength, Vb max} = 4414.6\ \text{kN}$$

(b) Steel frame:

$$\text{Maximum strength, Vb max} = 3432.5\ \text{kN} \tag{11}$$

From the calculations, the overall lateral stiffness, ductility, and strength of the composite frame are found to be greater than those of the steel frame.

From the graph in Figure 17, the maximum monitored top story displacement at the time of the collapse of the composite frame and steel frame are 633.79 mm and 563.90 mm, respectively.

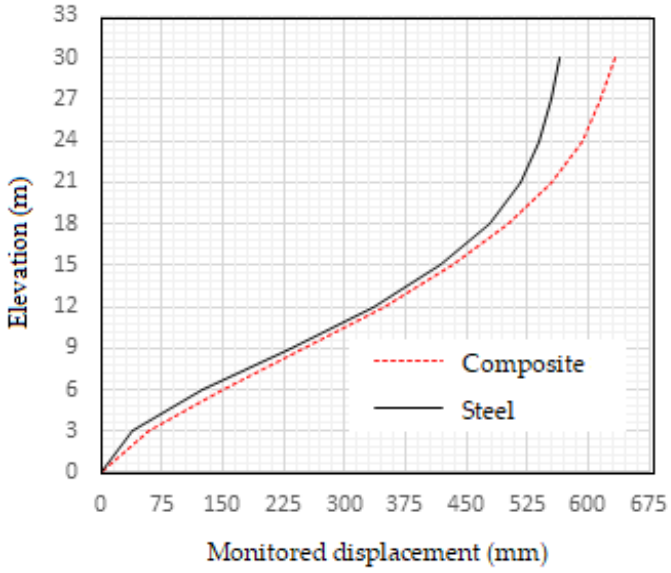

Figure 17. Maximum monitored displacement. Elevation (m).

From the graph in Figure 18, it is observed that maximum story drifts are experienced on the third and fourth floors, respectively. As a consequence of this, a greater number of severe hinges is found to be formed between the third and fourth floors in both the steel and composite frames. The maximum drifts experienced by steel and composite frames are 0.036 and 0.033, respectively.

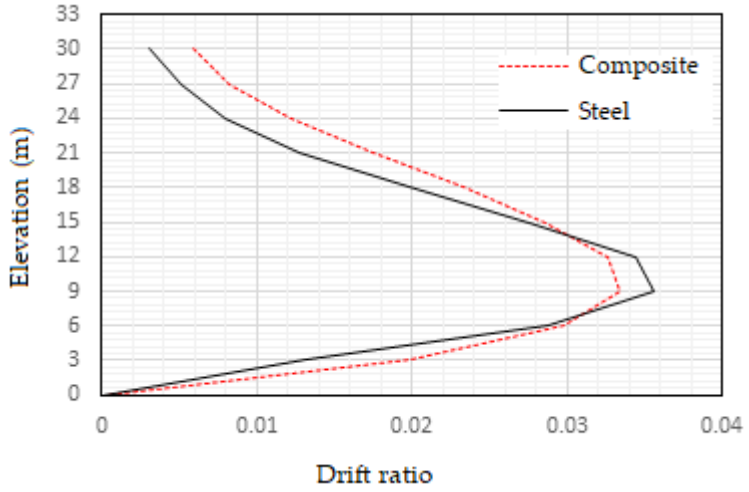

Figure 18. Maximum story drifts with respect to elevation.

4.7. Moment Rotation Curves

B14H18 and C9H17 Comparison

Since story drift is maximum on the third-floor level, more severe hinges were formed here. Hence, from the third floor, for a monitored displacement of 563.9 mm, moment values of two adjacent hinges from Beam number 14 and Column number 9 are compared here. Column 9 comes directly below Beam number 14. Before the failure, the hinge in the steel beam was subjected to a moment of 205.51 kNm and underwent a rotation of 0.032 rad, whereas the hinge in the composite beam reached a lesser moment of 201.33 kNm and rotation of 0.027 rad, which prevented it from completely failing. It is observed that the moment taken up by the C9H17 hinge in the composite frame is 547.5 kNm and that in the steel frame is 463.4 kNm. This indicates that the column in the composite frame attracted more load toward it owing to its greater stiffness and prevented the failure of the beam. A

similar trend is observed throughout the composite frame, which, in effect, reduced the number of hinges in the composite frame compared to the steel frame. The hinge details are shown in Tables 10–12. Figure 19 shows the formation of hinges for steel and composite. Red circles indicate hinges formed at maximum moments and failure indicating greater stiffness. The moment-rotation curves are shown in Figure 20. The selected hinges are shown below.

The column hinges at the base story are compared here. The maximum moment taken by columns in the composite frame before the failure of the structure is greater than that of steel frame columns before its failure indicating its greater stiffness.

Table 10. Moment-rotation values of beam hinge B14H18.

Hinge Number	Frame	Moment, M3 (kN-m)	Hinge State	Hinge Level	Rotation (rad)
B14H18	Composite	201.3	B to ≤C	LS to ≤CP	0.027
	Steel	0	>E	>CP	0.047

Table 11. Moment-rotation values of column hinge C9H17.

Hinge Number	Frame	Moment, M3 (kN-m)	Hinge State	Hinge Level	Rotation (rad)	Axial Force (kN)
C9H17	Composite	547.5	A to ≤B	A to ≤IO	0.0008	547.5
	Steel	463.4	A to ≤B	A to ≤IO	0	463.4

Table 12. Moment-rotation values of column hinge C6H1.

Hinge Number	Frame	Moment, M3 (kN-m)	Hinge State	Hinge Level	Rotation (rad)	Axial Force (kN)
C6H1	Composite	1761.5	B to ≤C	LS to ≤CP	0.0067	1409.5
	Steel	1317.4	A to ≤B	A to ≤IO	0	1217.1

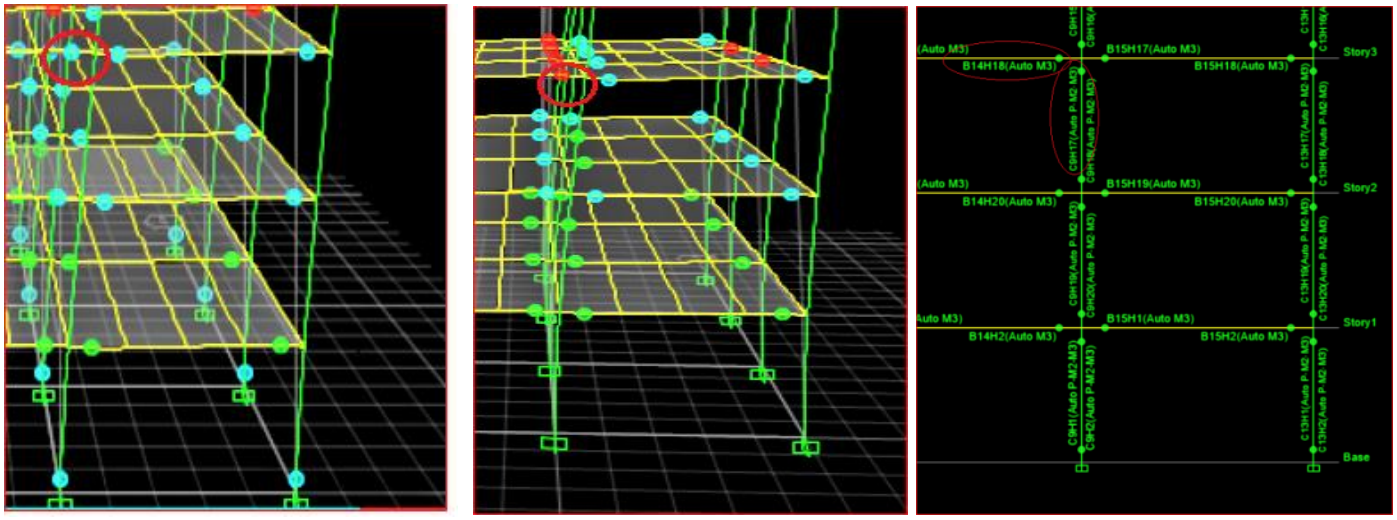

(**a**) (**b**) (**c**)

Figure 19. Formation of hinges for composite and steel frames. (**a**) Composite frame. (**b**) Steel frame. (**c**) Hinges considered.

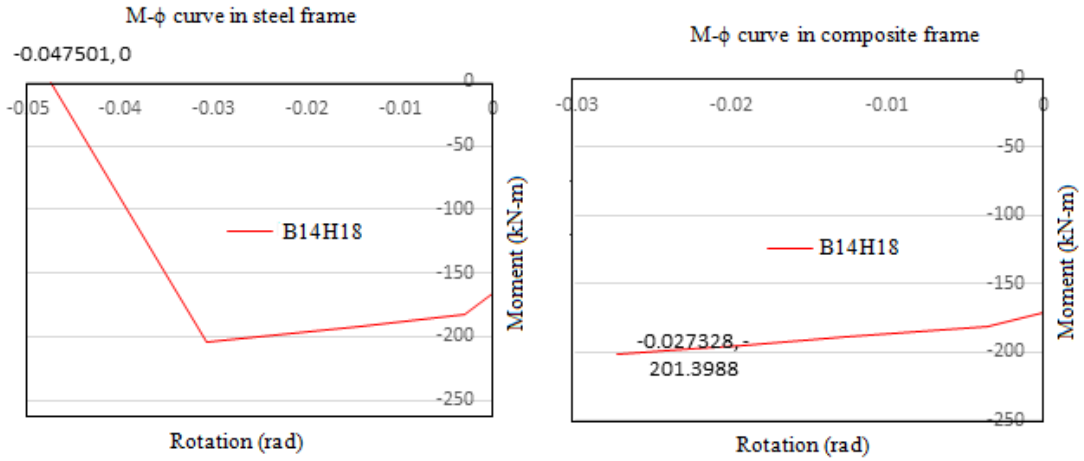

Figure 20. M-ϕ curve of B14H18 in steel frame (at d = 563.9 mm) and composite frame (at d = 563.9 mm).

4.8. Time History Analysis

The nonlinear direct integration time history analysis has been performed along the horizontal *x*-direction on both steel and composite frames, respectively. The time histories for dynamic analysis in this study were taken from Pacific Earthquake Engineering Research (PEER) ground motion database. Two near-field and two far-field ground motions were selected for the comparative study. PEER database has the option to filter and do ground motion scaling online. The design spectrum of IS1893:2002 for Site II, Seismic zone V, and damping of 5% is used as the target spectrum. For the selection of ground motions, epicentral distances of 0–15 km and 50–150 km were given for near-field and far-field earthquakes, respectively. In order to keep the scale factor from becoming too high or too low, the range of scale factor was given as 0.5–2.0 so that the selected ground motions did not have huge variations from the IS target spectrum. The period points were given as 0.47, 1, 3.7 (0.2–1.5 T).

4.9. Earthquake Details

The earthquakes which occur in fields near the fault are called near-field earthquakes. There is still disagreement among researchers on which range should an earthquake be considered as near-field. Many suggest a range of up to 10–60 km around the fault as the near-field range. According to the UBC-97 code, a distance less than 15 km from the epicenter is in the near-field range. The details of the time histories are given in Table 13.

Table 13. Earthquake details.

Earthquake Name	Year	Station Name	Mechanism	Type	Magnitude Mw	Epicentral Distance Rrup (km)	Vs (m/s)
Kocaeli, Turkey	1999	Izmit	Strike-Slip	Near-Field	7.51	7.21	811
Duzce, Turkey	1999	IRIGM496	Strike-Slip	Near-Field	7.14	7.14	760
Landers	1992	Palm Springs Airport	Strike-Slip	Far-Field	7.28	159.13	315.06
Big Bear-01	1992	LA-NWestmoreland	Strike-Slip	Far-Field	6.46	51.51	312.47

The accelerations are given in "g".

The analysis results are shown in the sections below.

For Kocaeli (near-field) Horizontal component 180°; Duration = 30 s; DT = 0.005 s; f = 0.125 Hz.

Further depending upon Kocaeli, Duzce, Landers and Big Bear earthquake data Figures 21–24 represents accelerogram, Base shear time history, Displacement time history for composite and steel frame. Also displacement, energy dissipated acceleration time history, maximum story displacement and Maximum story drift are plotted.

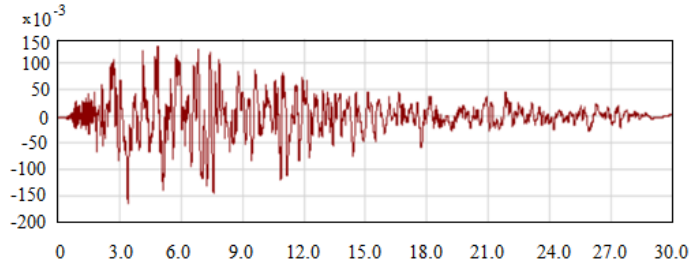

(a)

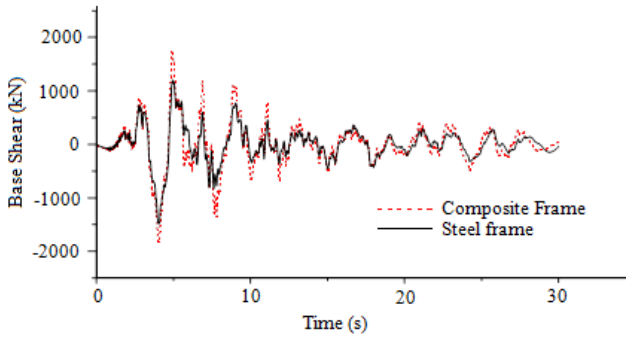

(b)

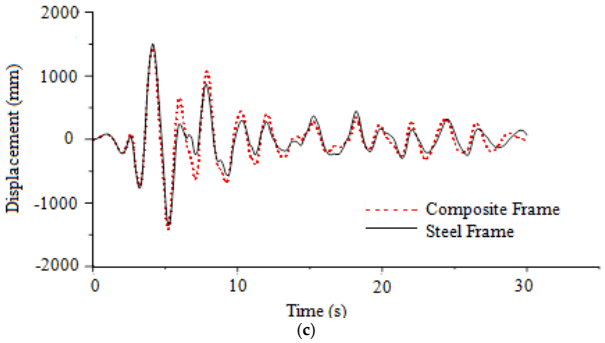

(c)

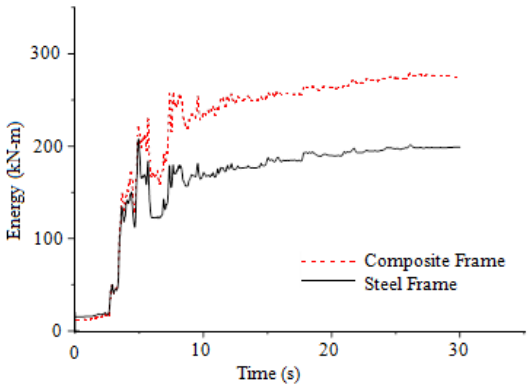

(d)

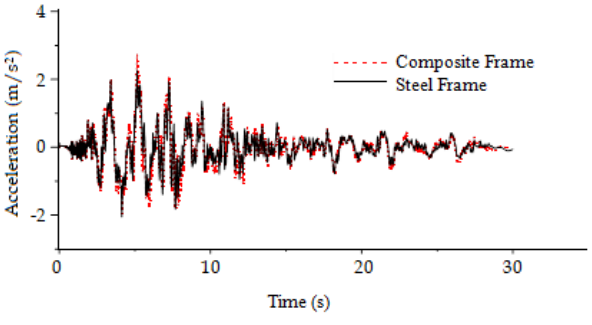

(e)

Figure 21. *Cont.*

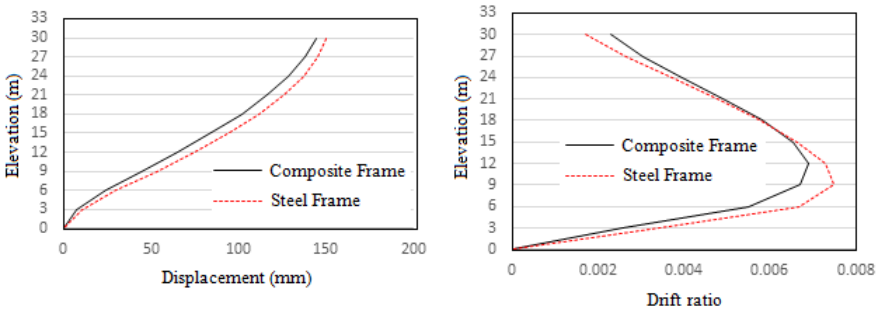

(**f**)

Figure 21. (**a**) Kocaeli accelerogram. (**b**) Base shear time history. (**c**) Displacement time history. Composite Frame, Steel Frame, Displacement (mm). (**d**) Energy dissipated. (**e**) Acceleration time history. (**f**) Maximum story displacement and Maximum story drift plot.

For Duzce (Near-field), Horizontal component 180°, Duration = 30.004, DT = 0.004 s, f = 0.0375 Hz.

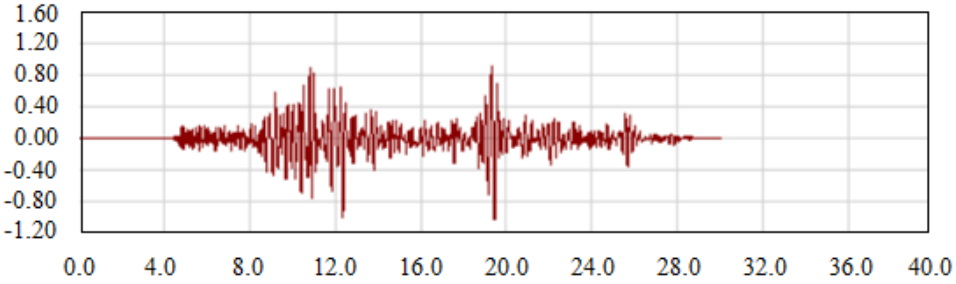

(**a**)

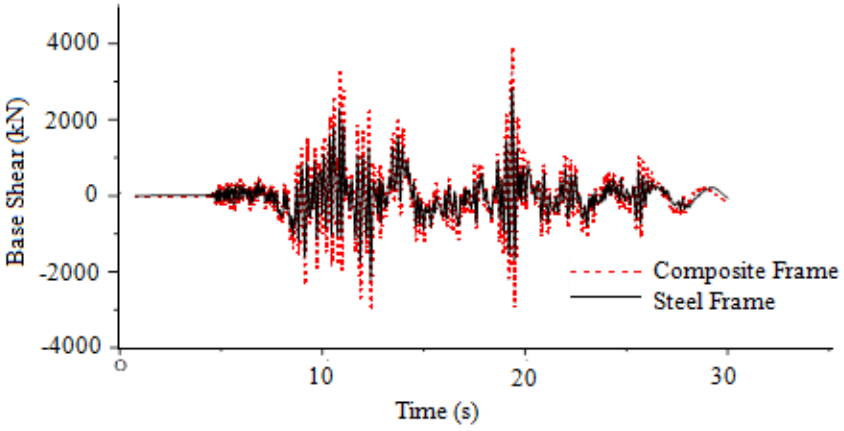

(**b**)

Figure 22. *Cont.*

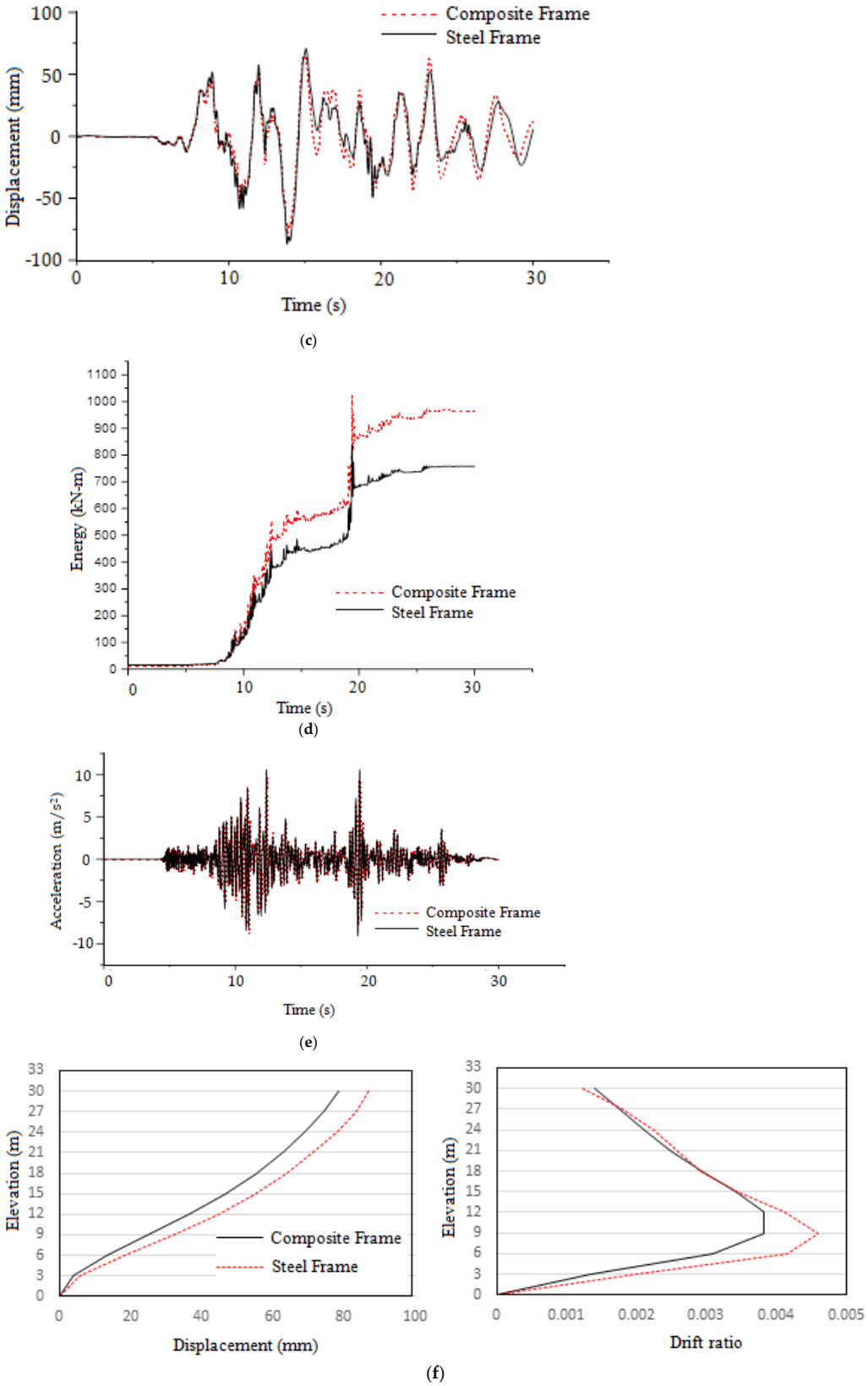

Figure 22. (**a**) Duzce accelerogram. (**b**) Base shear time history. (**c**) Displacement time history. (**d**) Energy dissipated. (**e**) Acceleration time history. (**f**) Maximum story displacement plot and Maximum story drift plot.

For Landers (Far-field), Horizontal component 0°, Duration = 39.655 s, DT = 0.005 s, f = 0.08 Hz.

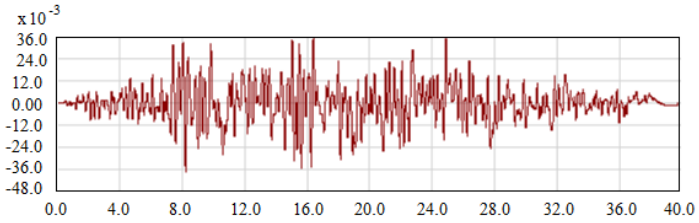

(**a**)

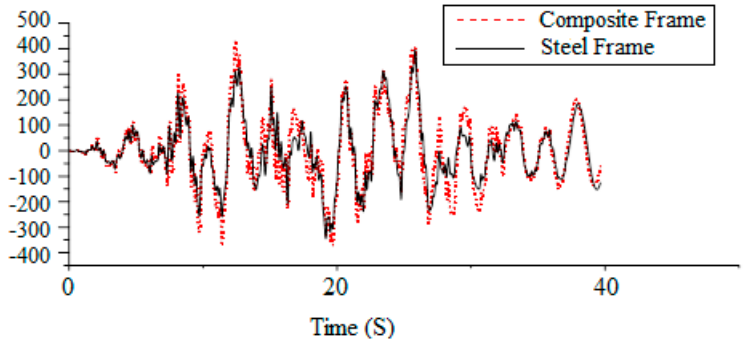

(**b**)

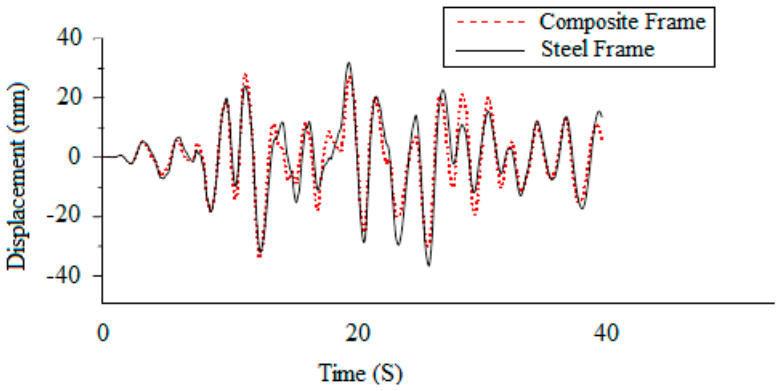

(**c**)

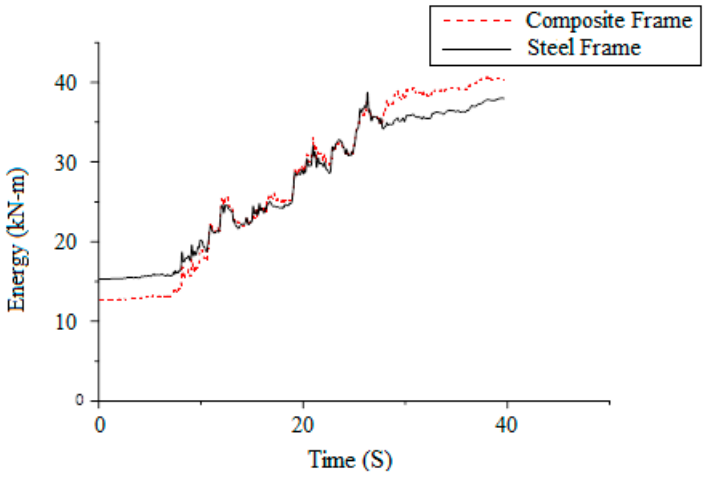

(**d**)

Figure 23. *Cont.*

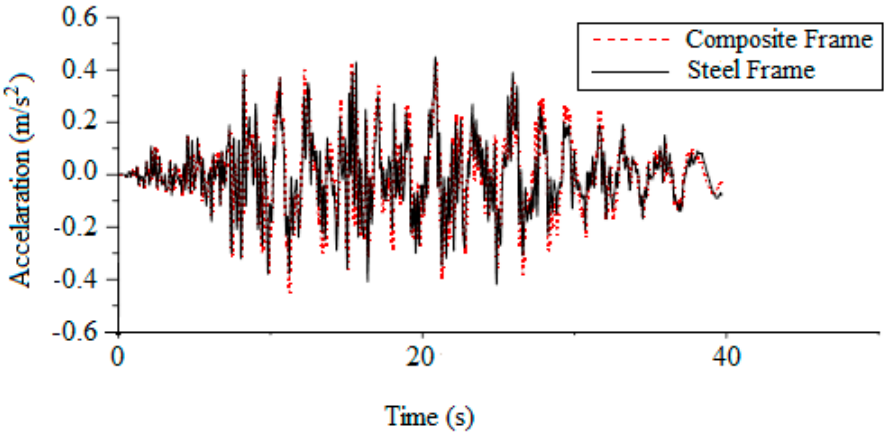

(**e**)

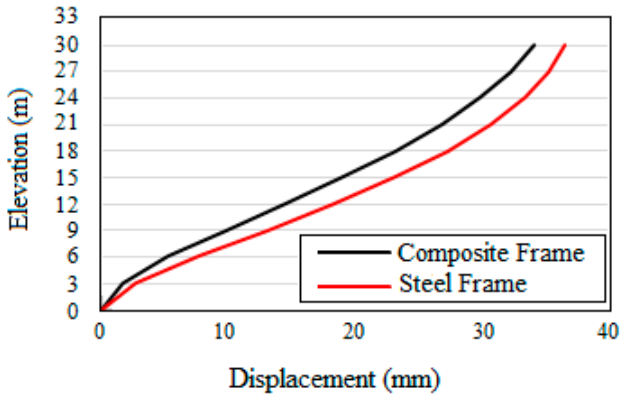

(**f**)

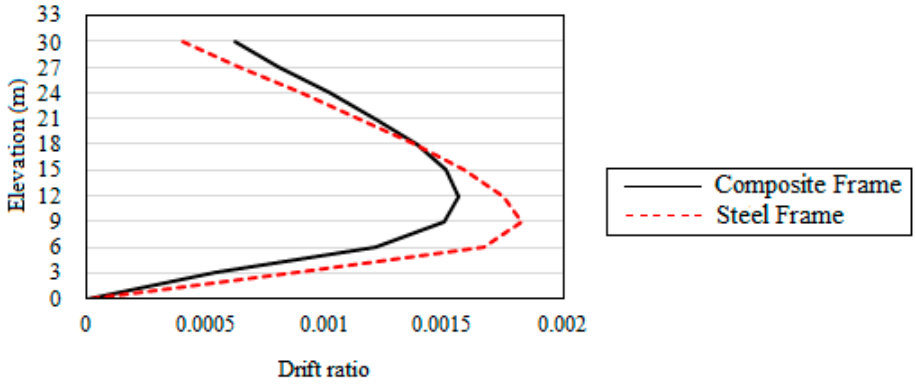

(**g**)

Figure 23. (**a**) Landers accelerogram. (**b**) Base shear time history. (**c**) Displacement time history. (**d**) Displacement time history. (**e**) Acceleration time history. (**f**) Maximum story displacement plot. (**g**) Maximum story drift plot.

For Bear (Far-field), Horizontal component 90°, Duration = 60 s, DT = 0.02 s, f = 0.24 Hz.

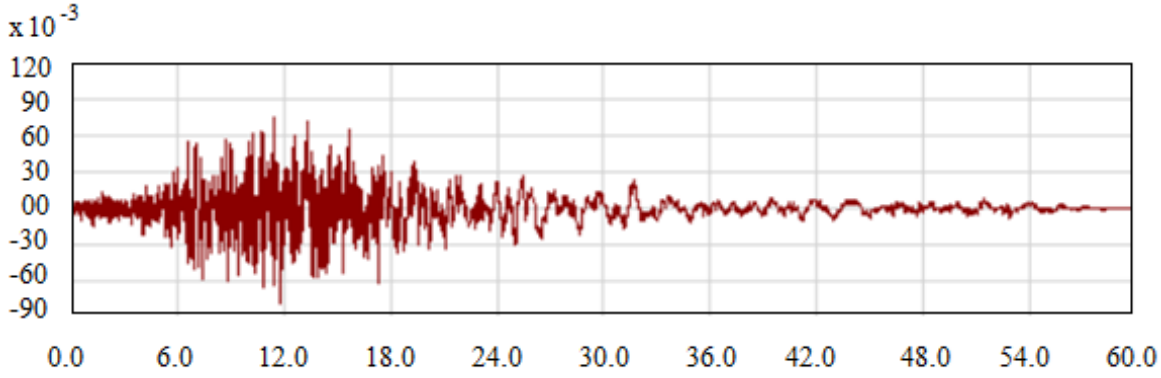

(**a**)

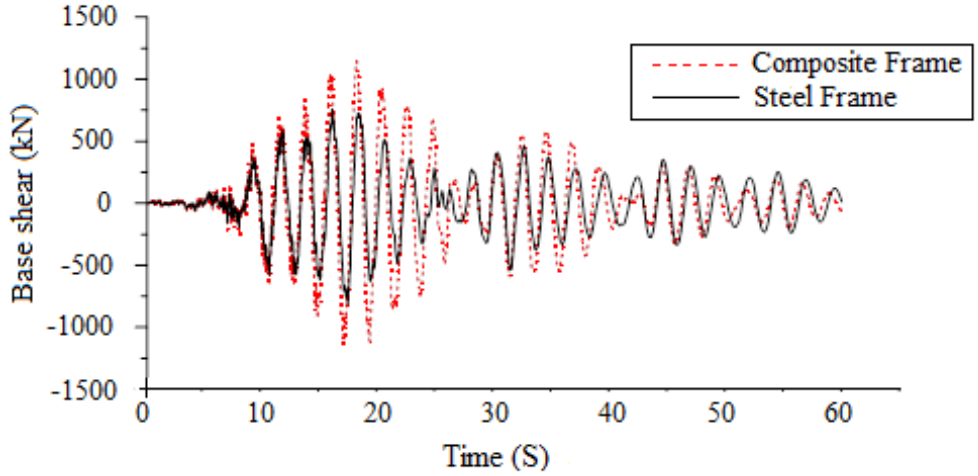

(**b**)

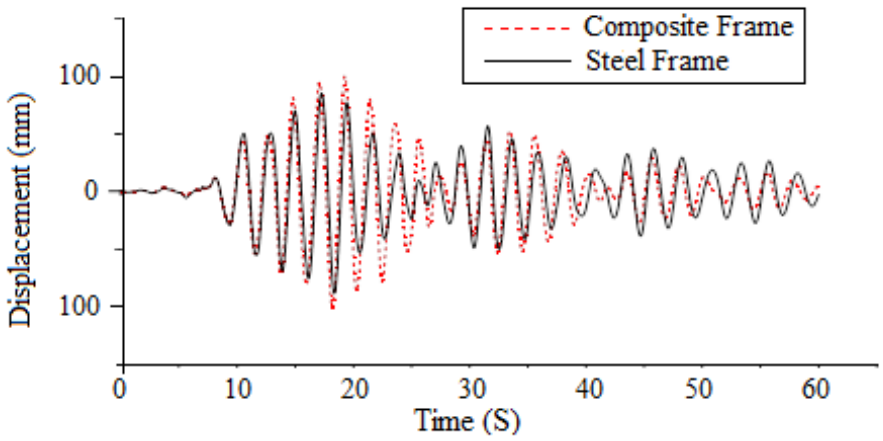

(**c**)

Figure 24. *Cont.*

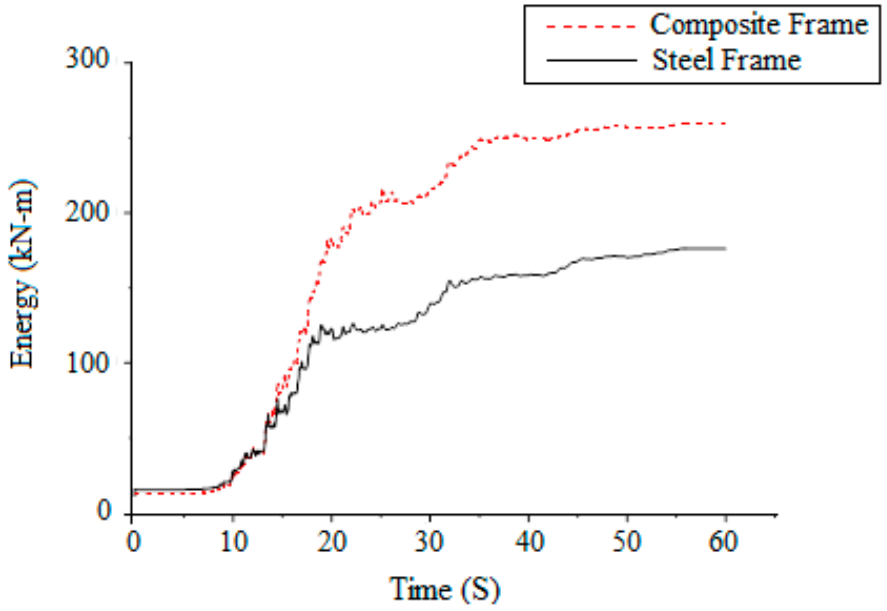

(**d**)

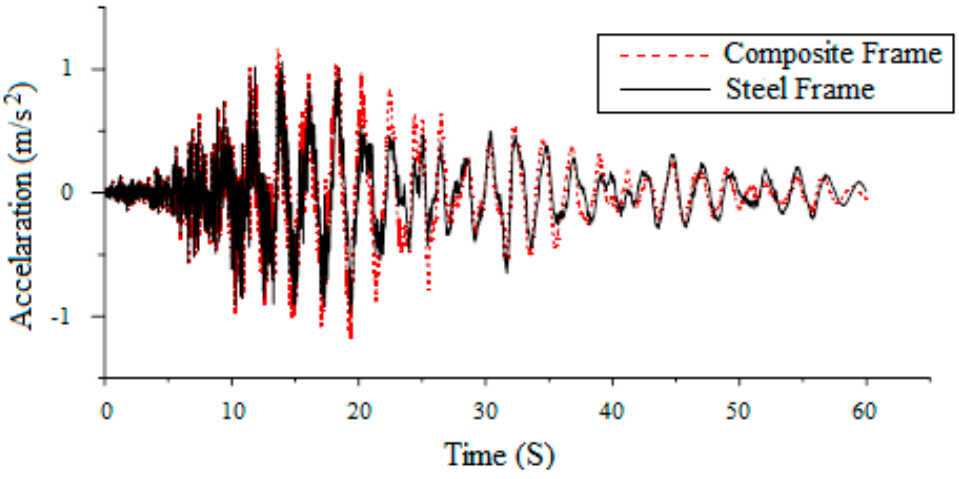

(**e**)

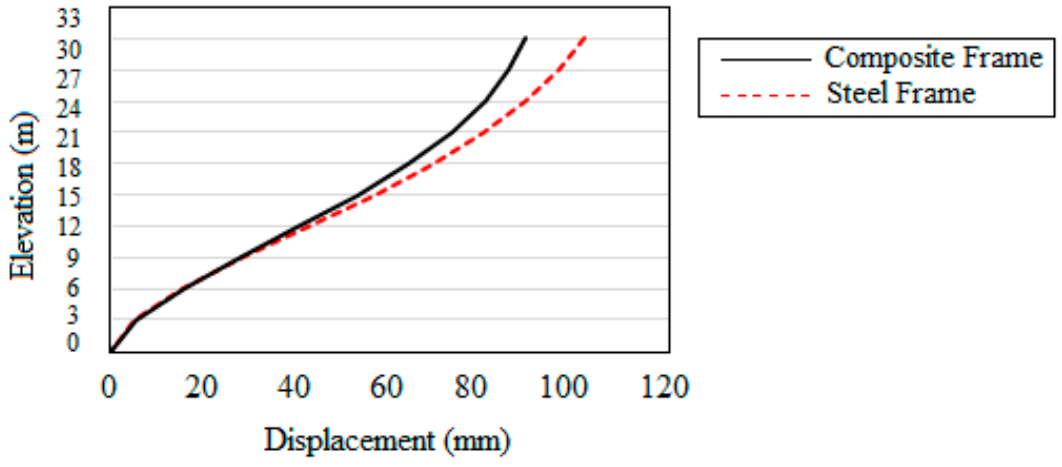

(**f**)

Figure 24. *Cont.*

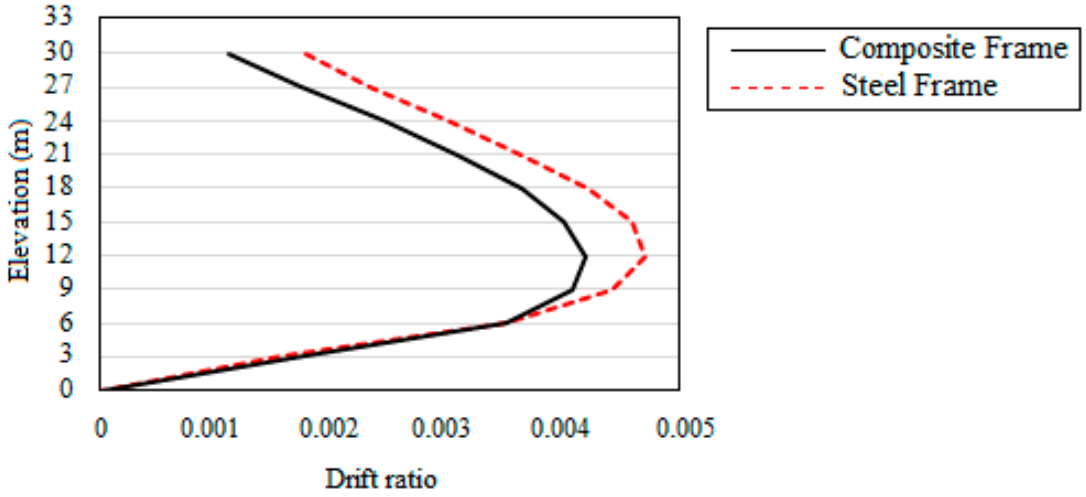

(**g**)

Figure 24. (**a**) Big Bear accelerogram. (**b**) Base shear time history. (**c**) Displacement time history. (**d**) Energy dissipated. (**e**) Acceleration time history. (**f**) Maximum story displacement plot. (**g**) Maximum story drift plot.

4.10. Comparison of Earthquake Responses

From the graphs obtained from nonlinear direct integration time history analysis, the maximum responses of both the composite and steel frames are compiled in Table 14.

Table 14. Comparison of maximum responses of frames.

Event	Frame Type	Top Story Displacement (mm)	Drift Ratio	Base Shear (kN)	Joint Acceleration (m/s^2)	Energy (kN-m)
Kocaeli (Near-field)	Composite	144.54	0.0069	1837.8	2.75	279.16
	Steel	150.38	0.0075	1488.35	2.26	207.94
Duzce (Near-field)	Composite	78.60	0.0038	3943.91	10.55	1022.11
	Steel	87.08	0.0046	2819.54	10.61	836.73
Landers (Far-field)	Composite	34.21	0.0016	434.48	0.449	40.68
	Steel	36.59	0.0018	395.13	0.445	38.77
Big Bear (Far-field)	Composite	101.37	0.0047	1145.46	1.18	259.80
	Steel	88.86	0.0042	816.76	1.06	176.35

From Table 14, it is clear that the displacement and story drifts are greater for the steel frame compared to the composite frame. However, the displacement and drift values are found to be more dependent on the frequency of the earthquakes and how much closer it is to the natural frequency of the frames. It is evident from the table that even though Duzce is a near-field earthquake, its displacement and drift values on the frames are lesser than those of the far-field earthquake Big Bear. The reason for this is that the frequency of Big Bear 0.24 Hz is closer to the natural frequencies of steel and composite frame 0.40 Hz and 0.44 Hz, respectively, whereas the frequency of Duzce is 0.0375 Hz, which is not close to the natural frequency of either frame. The frequency of Kocaeli is 0.13 Hz, which again is closer to the natural frequency of frames and, hence, has greater displacement and drift values as well. The frequency of Landers 0.08 Hz is not close to the natural frequencies of the frames and, hence, has lesser responses. The above-said differences in values of displacement and drifts are due to the effect of resonance.

The other three responses, such as base shear, joint acceleration, and energy dissipation, are greater for the composite frame compared to the steel frame, probably owing to its greater mass and stiffness. From Table 14, it is also evident that the base shear, joint acceleration, and energy dissipated are greater for the near-field earthquakes compared

to the far-field earthquakes, probably because of the close proximity of frames to the earthquake epicenter. The near-field earthquakes have, therefore, released more energy to both frames than far-field earthquakes.

It can be inferred from the results that the overall response and damage of the frames due to the earthquake depends on two main factors, specifically, the frequency of the earthquake and the proximity of the epicenter to the site where buildings are located. A combination of these two factors defines the extent of damage the building undergoes due to the earthquake.

4.11. Comparison of Column Hinge C6H1 at Base Story

The column hinge C6H1 at the base story is compared here. The maximum moment and rotation undergone by this column in composite and steel frames are shown in Table 15.

Table 15. Comparison of Moment-rotation values of column hinge C6H1 for different EQ Event.

Event	Frame Type	Moment, M3 (kN-m)	Rotation, Φ (rad)	Axial Force, P (kN)	Hinge Level
Duzce (Near-field)	Composite Steel	568.65 403.58	0.00078 0	1414.54 1234.40	A to ≤IO A to ≤IO
Kocaeli (Near-field)	Composite Steel	548.78 357.35	0.00074 0	1408.62 1216.73	A to ≤IO A to ≤IO
Landers (Far-field)	Composite Steel	123.48 91.87	0.00013 0	1413.29 1235.60	A to ≤IO A to ≤IO
Big Bear (Far-field)	Composite Steel	353.31 187.25	0.0039 0	1414.70 1223.38	A to ≤IO A to ≤IO

It is observed that the column hinges in both frames have remained within the immediate occupancy level safety throughout the ground excitation periods of all selected earthquakes. However, the composite column underwent slight rotation and took more moment compared to the steel frame. Similar to what was observed in the pushover analysis, the same trend is being observed here. This additional stiffness of the composite frame has significantly reduced the number of severe hinges formed, and thus, it has a role in prolonging its ability to withstand critical collapse damages. Moreover, the values indicate that both frames have experienced greater moments and rotations in the case of near-field earthquakes than far-field earthquakes.

4.12. Quantity of Materials Comparison

Composite frame requires 21 percent less structural steel compared to steel frame. Nevertheless, it needs 85 percent more concrete and an additional 6 percent Fe 415 reinforcement bars with respect to the structural steel required in the steel frame. The quantities of materials for steel and composite frames are shown in Figure 25a,b and Table 16.

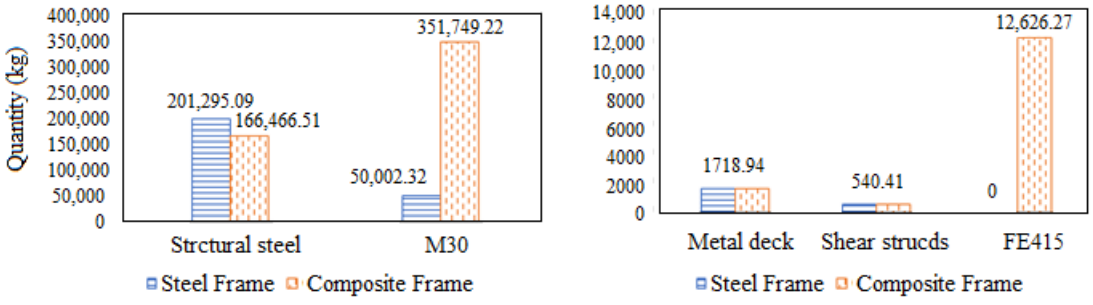

(**a**) (**b**)

Figure 25. (**a**) Quantity of structural steel and concrete. (**b**) Quantity of metal deck, shear studs, and Fe415.

Table 16. Quantity of materials.

Materials	Quantity (kg)	
	Composite	Steel
Structural steel	166,466.51	201,295.09
M30	351,749.22	50,002.32
Metal deck	1718.94	1718.94
Shear studs	540.41	540.41
Fe 415	12,626.27	0

5. Conclusions

The present work extends the comparative analysis of steel and composite frames with respect to inelastic behavior under earthquake excitations. It can be inferred from the current research that the overall inelastic performance of the composite frames is superior to the steel frames for the same plastic moment capacity of sections. The following points summarize the concluding remarks drawn from this study:

- The results from response spectrum analysis show that the displacements and drifts are greater in steel frames, and the responses such as story shears, overturning moments, and story stiffness are greater in composite frames;
- From the idealized capacity curve, the stiffness of the composite frame is 21.5% higher in the elastic region and 41.2% higher in the nonlinear region initially, and 5.5% higher when nearing collapse than that of the steel frame;
- The ductility ratio of the composite frame is 2.75, and that of the steel frame is 2.56. The lateral strength of the composite frame from the idealized capacity curve is 4414.6 kN, and that of the steel frame is 3432.5 kN. Furthermore, the maximum base shear value in the composite frame is 22.3% higher than that of the steel frame;
- The steel frame has an 8.4% higher story drift than the composite frame;
- The performance points using the capacity spectrum method for steel and composite frames as per IS1893:2002 are (2875.25 kN, 320.74 mm) and (3733.57, 312.26 mm), respectively, for the design-based earthquake (DBE);
- The target displacement points using the displacement coefficient method for steel and composite frames as per IS1893:2002 are (2954.46 kN, 344.01 mm) and (3787.86 kN, 322.69 mm), respectively, for a design-based earthquake (DBE);
- From time history analysis, it is concluded that the displacement and drift values are found to be more dependent on the frequency of the earthquakes and how close they are to the natural frequency of the frames due to the effect of resonance. The closer the frequencies, the greater the response;
- The composite frame requires 21% less structural steel compared to the steel frame and 85% more concrete compared to the steel frame. In addition, the composite frame requires 6% more steel for the Fe415 rebars.

Author Contributions: Formation of the original draft, conceptualization, and validation is performed by P.D.G.; reviewing the original draft and preparation are performed by N.S.M.; methodology, resources, and data creation are performed by V.B.; writing, review, and editing are performed by R.L.W.; analysis, model making, and comparison of the results are performed by S.P.V. All authors have read and agreed to the published version of the manuscript.

Funding: This research received no external funding.

Data Availability Statement: Data may be available on request.

Conflicts of Interest: The authors declare no conflict of interest.

References

1. Whittaker, A.; Constantnou, M.; Tsopelas, P. Displacement Estimates for Performance Based Seismic Design. *J. Struct. Div. ASCE* **1998**, *124*, 905–912. [CrossRef]
2. Architectural Institute of Japan (AIJ). *Structural Calculations of Steel Reinforced Concrete Structures*; Architectural Institute of Japan (AIJ): Tokyo, Japan, 1987.

3. American Institute of Steel Construction (AISC). *Load and Resistance Factor Design Specification for Structural Steel Buildings*; AISC: Chicago, IL, USA, 1999.
4. Ghobarah, A.; Abou-Elfath, H.; Biddah, A. Response-Based Damage Assessment of Structures. *Earthq. Eng. Eng. Seismol.* **1999**, *28*, 79–104. [CrossRef]
5. Chopra, A.K.; Chintanapakdee, C. Comparing response of SDF Systems to Near-Fault and Far-Fault Earthquake Motions in the Context of Spectral Regions. *Earthq. Eng. Struct. Dyn.* **2001**, *30*, 1769–1789. [CrossRef]
6. Xue, Q. A Direct Displacement Based Seismic Design Procedure of Inelastic Structures. *Eng. Struct.* **2001**, *23*, 1453–1460. [CrossRef]
7. Elenas, A.; Meskouris, K. Correlation study between seismic acceleration parameters and damage indices of structures. *Eng. Struct.* **2001**, *23*, 698–704. [CrossRef]
8. *IS 1893*; Indian Code for Earthquake Resistant Structures. Bureau of Indian Standards: New Delhi, India, 2002.
9. *IS 12778*; Indian Standard Code of Practice for Hot Rolled Parallel Flange Steel Sections for Beams, Columns and Bearing Piles—Dimensions and Section Properties. Bureau of Indian Standards: New Delhi, India, 2004.
10. Oh, M.; Ju, Y.; Kim, M.; Kim, S. Structural Performance of Steel-Concrete Composite Column Subjected to Axial and Flexural Loading. *J. Asian Archit. Build. Eng.* **2006**, *5*, 153–160. [CrossRef]
11. *IS 800*; Indian Standard Code of Practice for General Construction in Steel. Bureau of Indian Standards: New Delhi, India, 2007.
12. Mohd, Y.A.Y.; David, A.N. Cross-sectional properties of complex composite beams. *Eng. Struct.* **2007**, *29*, 195–212. [CrossRef]
13. Gewei, Z.; Basu, B. A study on friction-tuned mass damper: Harmonic solution and statistical linearization. *J. Vib. Control* **2010**, *17*, 721–731. [CrossRef]
14. Sayani, P.J.; Erduran, E.; Ryan, K.L. Comparative response assessment of minimally compliant low-rise base isolated and conventional steel moment resisting frame buildings. *J. Struct. Eng. ASCE* **2011**, *137*, 1118–1131. [CrossRef]
15. Gray, B.M.; Christopoulos, C.; Eng, P.; Packer, J.; Gray, M. A New Brace Option for Ductile Braced Frames. *Mod. Steel Constr.* **2012**, 40–43. Available online: https://www.aisc.org/globalassets/modern-steel/archives/2012/02/2012v02_new_brace.pdf (accessed on 5 July 2023).
16. Wankhade, R.L.; Landage, A.B. Static Analysis For Fixed Base And Base Isolated Building Frame. In Proceedings of the National Conference on Advances in Civil and Structural Engineering (NCACSE-2014), Karad, India, 18–19 April 2014.
17. Wankhade, R.L. Performance Based Design and Estimation of Forces for Building Frames with Earthquake Loading. In Proceedings of the International Conference on Recent Trends and Challenges in Civil Engineering, Allahabad, India, 12–14 December 2014; MNNIT Allahabad: Allahabad, India, 2014.
18. Wankhade, R.L.; Landage, A.B. Performance Based Analysis and Design of Building Frames with Earthquake Loading. *Int. J. Eng. Res.* **2016**, *5*, 106–110.
19. Wankhade, R.L. Performance Analysis of RC Moment Resisting Frames Using Different Rubber Bearing Base Isolation Techniques. In Proceedings of the International Conference on Innovations in Concrete for Infrastructure Challenges, Nagpur, India, 6–7 October 2017.
20. Titikesh, A.; Bhatt, G. Optimum positioning of shear walls for minimizing the effects of lateral forces in multistorey buildings. *Arch. Civ. Eng.* **2017**, *63*, 151–162. [CrossRef]
21. Bazarchi, E.; Hosseinzadeh, Y.; Panjebashi, A.P. Investigating the in-plane flexibility of steel-deck composite floors in steel structures. *Int. J. Struct. Integr.* **2018**, *9*, 705–720. [CrossRef]
22. Boukhalkhal, S.H.; Jhaddoudene, A.N.T.; Neves, L.F.D.C.; de Silva, V.P.C.G.; Madi, W. Performance assessment of steel structures with semi-rigid joints in seismic areas. *Int. J. Struct. Integr.* **2019**, *11*, 13–28.
23. Nayak, C.B.; Jagadale, U.T.; Jadhav, K.M.; Morkhade, S.G.; Kate, G.K.; Thakare, S.B.; Wankhade, R.L. Experimental, analytical and numerical performance of RC beams with V-shaped reinforcement. *Innov. Infrastruct. Solut.* **2021**, *6*, 2. [CrossRef]
24. Wankhade, R.L.; Sawarkar, A.; Chandwani, A.; Chavan, S.; Malkar, P.; Sawarkar, G. Seismic Fragility of Buildings Subjected to Pounding Effects with Soil–Structure Interaction. In *Advances in Construction Materials and Sustainable Environment*; Gupta, A.K., Shukla, S.K., Azamathulla, H., Eds.; Lecture Notes in Civil Engineering; Springer: Singapore, 2022; Volume 196. [CrossRef]
25. Miani, M.; Di Marco, C.; Frappa, G.; Pauletta, M. Effects of Dissipative Systems on the Seismic Behavior of Irregular Buildings–Two Case Studies. *Buildings* **2020**, *10*, 202. [CrossRef]
26. Frappa, G.; Pauletta, M. Seismic retrofitting of a reinforced concrete building with strongly different stiffness in the main directions. In Proceedings of the 14th fib International Ph.D. Symposium in Civil Engineering, Rome, Italy, 5–7 September 2022.
27. Mo, Z.; Feng, Q.; Lai, B.; Jiang, W.; Feng, Y. Resilient performance of super-elastic SMA bolted connection equipped with extended end plate and shear tab. *J. Constr. Steel Res.* **2022**, *199*, 107626. [CrossRef]
28. Lai, B.; Tan, W.; Feng, Q.; Venkateshwaran, A. Numerical parametric study on the uniaxial and biaxial compressive behavior of H-shaped steel reinforced concrete composite beam-columns. *Adv. Struct. Eng.* **2022**, *25*, 2641–2661. [CrossRef]